

Endothelial FUNDC1 regulates metabolic reprogramming and the obesity-diabetes transition through the SIRT3/GATA2/endothelin-1 axis

Received: 4 June 2025

Accepted: 11 January 2026

Published online: 16 January 2026

 Check for updatesJian Li^{1,4}, Dayong Li^{2,4}, Fujie Zhao^{1,4}, Yadong Wang¹, Hongmin Yao¹, Yin Wu¹, Junqing An¹, Zhixue Liu¹, Ye Ding¹✉ & Ming-Hui Zou³✉

Endothelial cell (EC) dysfunction is a hallmark of obesity and Type 2 diabetes mellitus (T2DM), yet the mechanisms linking vascular stress to systemic metabolic diseases remain unclear. Here, we investigated the role of the mitochondrial protein FUN14 domain-containing 1 (FUNDC1) in EC under nutritional overload. Using high-fat diet (HFD)-fed EC-specific *Fundc1* knock-out mice, human umbilical vein ECs, primary ECs, and vascular tissues from patients with obese/T2DM, we find that endothelial FUNDC1 expression is elevated under diabetic conditions, whereas its deletion protects mice from HFD-induced obesity, insulin resistance, and metabolic disorders. Mechanistically, overnutrition triggers nuclear export of the long isoform of SIRT3 (SIRT3-L) to mitochondria via FUNDC1, disinhibiting GATA2 and enhancing endothelin-1 (ET-1) production. Loss of FUNDC1 in ECs retains SIRT3-L in the nucleus, promoting GATA2 degradation and reducing ET-1. Endothelial FUNDC1 levels correlated positively with plasma ET-1 in individuals with obesity/T2DM. These findings identify endothelial FUNDC1 as a key regulator of vasculature-metabolic organ cross talks and obesity-diabetes transition.

Cardiovascular diseases (CVDs) remain the leading cause of morbidity and mortality worldwide, accounting for an estimated 17.9 million deaths annually^{1,2}. Despite significant advances in medical interventions and preventative strategies, the burden of CVDs continues to escalate, underscoring the urgent need for deeper mechanistic insights into their pathogenesis. Among the earliest detectable events in the progression of both vascular and metabolic diseases is endothelial cell (EC) dysfunction³⁻⁵, a critical process characterized by impaired vasodilation, increased vascular permeability, and a pro-inflammatory state⁶⁻⁸. Emerging evidence suggests that endothelial dysfunction is intricately linked to aberrant increases in endothelin-1

(ET-1), a potent vasoconstrictive peptide⁹. Elevated ET-1 levels have been implicated not only in vascular remodeling and hypertension but also in broader systemic effects that exacerbate cardiovascular risk.

The endothelium, a monolayer of specialized cells lining the vasculature, plays a pivotal role in maintaining vascular homeostasis. Through the balanced secretion of vasodilators such as nitric oxide (NO) and vasoconstrictors like ET-1, ECs orchestrate vascular tone, barrier integrity, and anti-thrombotic properties¹⁰. However, in pathological states, this equilibrium is disrupted, leading to endothelial dysfunction. Aberrant ET-1 expression is a hallmark of this dysregulation, contributing to oxidative stress, inflammation, and vascular

¹Institute for Biomedical Sciences, Georgia State University, Atlanta, GA, USA. ²NHC Key Laboratory of Hormones and Development, Tianjin Key Laboratory of Metabolic Diseases, Chu Hsien-I Memorial Hospital & Tianjin Institute of Endocrinology, Tianjin Medical University, Tianjin, China. ³Department of Endocrinology and Metabolism, Tianjin Medical University General Hospital, Tianjin, China. ⁴These authors contributed equally: Jian Li, Dayong Li, Fujie Zhao.

✉ e-mail: yding5@gsu.edu; mhzou@tmu.edu.cn

smooth muscle cell proliferation¹¹. Importantly, the implications of ET-1 extend beyond the vasculature and into systemic metabolism. For decades, studies in both animals and humans have demonstrated that ET-1 signaling contributes to obesity and adipose tissue dysfunction by promoting adipocyte proliferation, impairing adipocyte differentiation, and inducing insulin resistance^{12–14}. Conversely, blocking ET-1 signaling, particularly through the ET-1B receptor, protects against features of metabolic syndrome, at least in part by enhancing FGF21 activity and elevating circulating free thyroxine¹⁵. These findings establish ET-1 as a key mediator of the crosstalk between endothelial dysfunction and metabolic imbalance.

Emerging data further suggest that endothelial dysfunction is not only a consequence but also a driver of obesity¹⁶, highlighting a complex bidirectional relationship. ECs have been shown to influence adipocyte development and function via paracrine signaling pathways, including the secretion of ET-1 and other adipokines^{12,17,18}. Dysregulated ECs signaling promotes chronic inflammation and impaired adipogenesis, leading to ectopic fat deposition and metabolic abnormalities¹⁹. Conversely, obesity exacerbates endothelial dysfunction by increasing systemic inflammation, insulin resistance, and circulating free fatty acids³. Despite these insights, the upstream mechanisms that control endothelial ET-1 production under metabolic stress, and how this regulation contributes to the progression from obesity to Type 2 diabetes, remain incompletely understood.

Recent studies have identified Fun-14 domain-containing protein 1 (FUNDC1) as a multifunctional regulator of mitochondrial biology in EC and other cell types^{20–22}, positioning it as a potential link between mitochondrial dysfunction and systemic metabolic diseases. Beyond its well-established role in mitophagy through direct interaction with LC3²³, FUNDC1 also maintains the structural and functional integrity of mitochondria-associated membranes (MAMs)²¹, where it participates in crosstalk between mitochondria and the endoplasmic reticulum. FUNDC1 further interacts with dynamin-related protein 1 (DRP1) to facilitate mitochondrial fission through mitochondrial fission 1 protein (FIS1)²¹, and it contributes to calcium homeostasis in part by regulating IP3R-mediated Ca²⁺ transfer at the MAM interface²². These diverse roles in mitochondrial quality control, dynamics, and signaling highlight FUNDC1 as a central node in maintaining mitochondrial health. Dysfunctional mitochondria in ECs can impair nutrient sensing and energy signaling pathways, exacerbating endothelial dysfunction. This, in turn, may disrupt EC-adipocyte communication and contribute to the pathogenesis of obesity. Despite its emerging significance, the precise role of FUNDC1 in linking mitochondrial health, endothelial dysfunction, and metabolic disorders remains poorly defined. Investigating this interface could yield novel insights into how EC mitochondrial dynamics influence obesity development and progression.

Several gaps in knowledge persist in this field. While the contribution of endothelial dysfunction to CVDs is well-recognized, its mechanistic links to metabolic diseases such as obesity are less defined. Specifically, the role of ET-1 as a mediator of EC-adipocyte crosstalk warrants further investigation. Additionally, while preclinical studies have demonstrated the impact of EC-derived factors on adipose tissue remodeling, their translational relevance in human physiology remains unclear. Understanding these relationships could uncover novel therapeutic targets aimed at mitigating both vascular and metabolic dysfunction.

In this study, we aim to address these gaps by exploring the interplay between endothelial dysfunction, ET-1 dysregulation, FUNDC1-mediated mitochondrial dynamics, and adipocyte development. Our results indicate that FUNDC1 in ECs via ET1 release regulates insulin sensitivity and adiposity in mice in vivo and that high fat diet (HFD) promotes insulin resistance and overweight by increasing FUNDC1 and consequent ET1 release from ECs. Our results provide a comprehensive framework that advances our understanding of the endothelium's role in linking cardiovascular and metabolic health.

Results

Endothelial dysfunction occurs prior to insulin resistance under overnutrition condition

To investigate the sequence of insulin resistance and endothelial dysfunction during fat tissue development, we fed male C57BL/6 mice with an HFD for 2 and 6 months, respectively. Body weight and fat percentage significantly increased in both the 2-month- and 6-month-HFD-treated mice compared to control mice fed a chow diet (CD) (Supplementary Fig. 1a, b). In the 2-month-HFD-fed mice, serum levels of triglycerides (TG), fasting blood glucose (GLU), and insulin were comparable to their counterparts in control mice. However, after 4 additional months of HFD treatment, these serum biochemical markers were significantly elevated (Supplementary Fig. 1c–e). Similarly, the 2-month-HFD-fed mice showed no significant changes in insulin sensitivity compared to those in CD-fed mice, whereas the 6-month-HFD-fed mice exhibited marked insulin resistance when compared to those in the 2-month-HFD-fed group (Supplementary Fig. 1f–i).

We also assessed endothelium function by evaluating aortic stiffness and vasodilatory response. As shown in Supplementary Fig. 1j–m, 2 months of HFD feeding impaired vascular stiffness, evidenced by reduced ascending aortic strain but increased pulse wave velocity (PWV). It also compromised endothelium-dependent vasodilation, as indicated by a decreased response to acetylcholine but not to sodium nitroprusside (SNP). In the 6-month-HFD-fed mice, while ascending aortic strain was further reduced compared to the 2-month-HFD-fed group, PWV remained unchanged, and no further impairment in vasodilatory response was observed. In addition, these results were further strengthened by the measurement of the phosphorylation of VASP at Ser239 (p-VASP Ser239), a well-established downstream marker of NO-cGMP signaling, in whole aortas from CD-fed mice, 2-month HFD, or 6-month HFD (Supplementary Fig. 1n, o). Consistent with the impaired acetylcholine-mediated vasorelaxation, we found that p-VASP Ser239 expression was significantly reduced in both the 2-month and 6-month HFD groups compared with chow controls, with no further reduction between 2 and 6 months. These results provide independent molecular evidence that EC NO signaling is already compromised at 2 months of HFD and does not deteriorate further at 6 months, in line with our functional data. Taken together, these data suggest that endothelial dysfunction occurs as early as 2 months after HFD feeding, preceding the onset of insulin resistance under conditions of overnutrition.

EC plays vital role in adipocyte differentiation and insulin sensitivity

Structurally, ECs form an extensive capillary network throughout the body, with a total length of approximately 0.9 m per mm³ of white adipose tissue (WAT). Each adipocyte is directly connected to the surrounding capillary network in a circular arrangement²⁴. Additionally, ECs constitute nearly 33% of the freshly isolated stromal vascular fraction (SVF) cells from WAT²⁵. To further investigate the functional importance of ECs in adipocyte development, we isolated CD31⁺ ECs-enriched fractions (CD31⁺ ECs) from SVF cells and examined both the differentiation rate of adipocytes and their insulin sensitivity. As shown in Supplementary Fig. 1p–r, the removal of CD31⁺ ECs significantly reduced the differentiation rate of adipocytes compared to SVF cells with intact CD31⁺ ECs, as evidenced by a decreased adipocyte number and a reduced Oil Red O-stained area.

Palmitic acid (PA) is a well-documented inducer of insulin resistance in adipocytes. Using this model, we evaluated the role of CD31⁺ ECs in insulin-stimulated 2-NBDG (a non-metabolizable fluorescent analogue of D-glucose) uptake. As shown in Supplementary Fig. 1s, in the presence of CD31⁺ ECs, PA caused a reduction in glucose uptake by approximately 59.9%. In contrast, the absence of CD31⁺ ECs mitigated this reduction to approximately 27.0%. Interestingly, under basal conditions treated with BSA, the removal of CD31⁺ ECs significantly

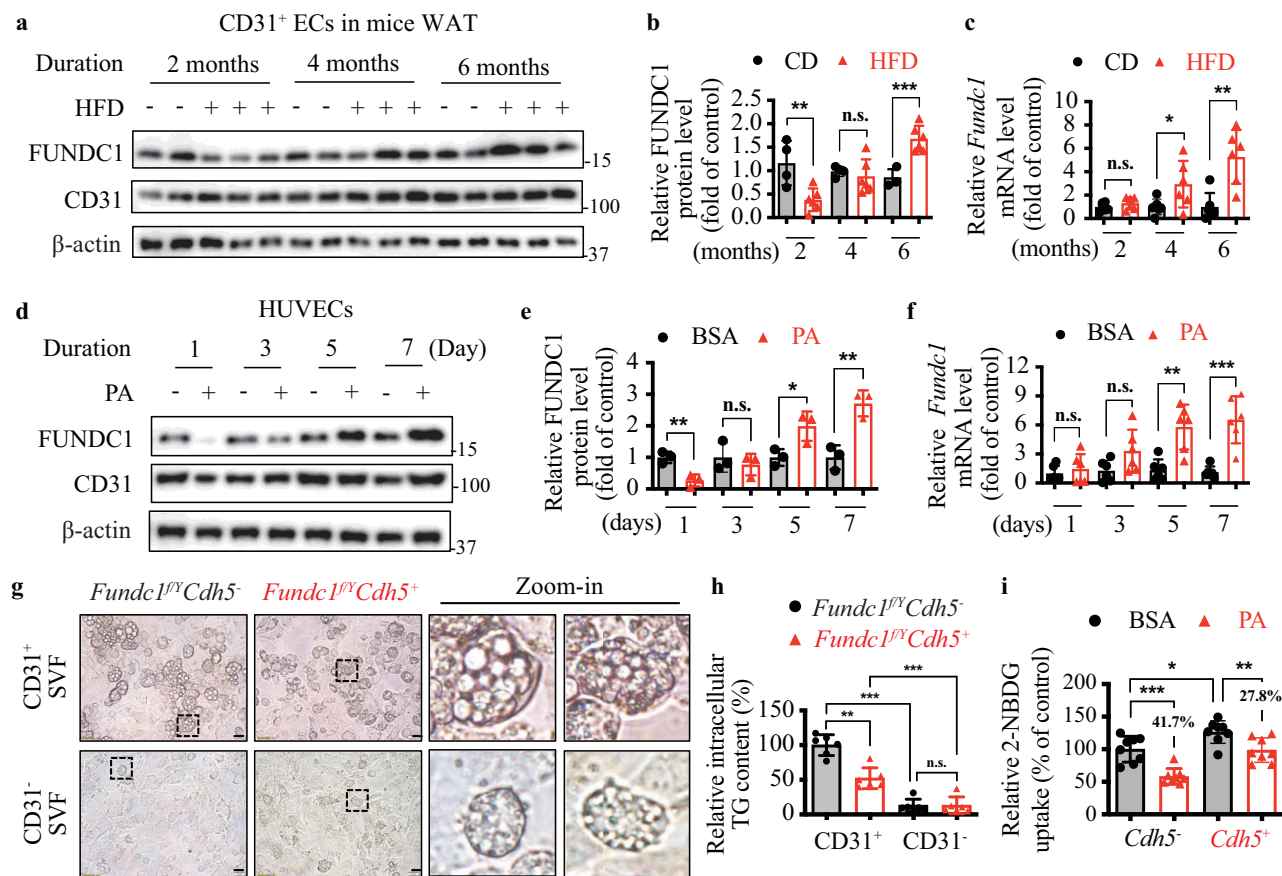


Fig. 1 | Endothelial FUNDC1 expression is dynamically regulated by metabolic stress and modulates adipocyte function and insulin sensitivity. **a–c** CD31 positive ECs (CD31⁺ ECs) were isolated from white adipose tissue (WAT) of mice fed with indicated durations (2, 4, 6 months) of HFD and subjected to western blot analysis ($n = 4$ mice/group) or Q-PCR analysis ($n = 6$ mice/group). **d–f** HUVECs were incubated with 200 μ M PA conjugated to fatty acid-free BSA, and culture medium containing PA or BSA was refreshed daily throughout the 7-day stimulation period to maintain a consistent lipid challenge. Cells were then subjected to western blot analysis or Q-PCR analysis. $n = 3$ independent experiments. **g** CD31 positive cells

were removed from the SVF of *Fundc1^{fl/y}Cdh5^{-/-}* or *Fundc1^{fl/y}Cdh5^{+/+}* mice (CD31⁻ SVF). Normal SVF containing CD31 positive cells was used as control (CD31⁺ SVF). Cells were then differentiated into adipocytes. Scale bar: 50 μ m. **h** Intracellular TG content in **(g)**. $n = 6$ independent experiments. **i** Insulin-stimulated 2-NBDG uptake in primary adipocytes isolated from *Fundc1^{fl/y}Cdh5^{-/-}* or *Fundc1^{fl/y}Cdh5^{+/+}* mice in the presence of bovine serum albumin (BSA) or palmitic acid (PA). $n = 8$ independent experiments. Data are presented as mean \pm SD. * $p < 0.05$, ** $p < 0.01$, *** $p < 0.001$, n.s. $p > 0.05$.

increased 2-NBDG uptake. Collectively, these findings highlight the functional importance of ECs in regulating adipocyte differentiation and insulin sensitivity.

Endothelial FUNDC1 dynamically regulated by metabolic stress modulates adipocyte function and insulin sensitivity

To investigate the dynamic regulation of endothelial FUNDC1 expression under metabolic stress, we first isolated CD31⁺ ECs from white adipose tissue (WAT) of mice fed with a HFD for 2, 4, or 6 months. To assess purity, we evaluated both CD31 (EC marker) and α -SMA (a marker for fibroblasts and smooth muscle cells). As shown in Supplementary Fig. 1t, α -SMA was highly expressed in whole aorta and isolated smooth muscle cells (used as positive controls) but was not detected in our ATEC preparations. In contrast, CD31 was robustly expressed in primary mouse adipose tissue endothelial cells (ATECs), confirming EC identity. Western blot analysis revealed a biphasic pattern of FUNDC1 protein expression: a significant reduction was observed at 2 months, no apparent change at 4 months, and a marked increase at 6 months (Fig. 1a, b). In contrast, quantitative PCR showed that FUNDC1 mRNA levels remained unchanged at 2 months but gradually increased at 4 and 6 months of HFD feeding (Fig. 1c), suggesting a post-transcriptional mechanism may account for early protein reduction. To model these changes in vitro, HUVECs were treated with

palmitic acid (PA, 200 μ M) for up to 7 days. FUNDC1 protein levels decreased after 1 day of PA exposure, returned to baseline by day 3, and were elevated at days 5 and 7 (Fig. 1d, e). Similarly, FUNDC1 mRNA expression was unchanged at days 1 and 3 but significantly increased at days 5 and 7 (Fig. 1f). These data imply that short-term metabolic stress suppresses FUNDC1 protein via enhanced degradation, while prolonged stress induces a compensatory transcriptional upregulation.

To investigate the direct role of reduced endothelial FUNDC1 in the development of T2DM, we generated *Fundc1^{fl/y}Cdh5^{-/-}* mice (Supplementary Fig. 2a). The knockout efficiency of the *Fundc1* gene was confirmed by immunofluorescence staining and western blot analysis of FUNDC1 protein expression in both ATECs and mouse lung endothelial cells (MLECs). As shown in Supplementary Fig. 2b–e, FUNDC1 protein expression was abolished in *Fundc1^{fl/y}Cdh5^{-/-}* mice, confirming specific deletion of *Fundc1* in ECs. Next, we prepared CD31 SVFs and CD31⁺ SVFs from *Fundc1^{fl/y}Cdh5^{-/-}* or *Fundc1^{fl/y}Cdh5^{+/+}* mice to evaluate their differentiation rate and insulin sensitivity. As depicted in Fig. 1g, h, CD31⁺ SVFs of *Fundc1^{fl/y}Cdh5^{-/-}* mice exhibited a significant reduction in the number of lipid droplets and displayed less PA-induced insulin resistance compared to CD31⁺ SVFs from *Fundc1^{fl/y}Cdh5^{+/+}* mice.

To assess the contributions of *Fundc1*-deficient ECs to adipocyte differentiation, we removed CD31⁺ cells from the SVFs of *Fundc1^{fl/y}Cdh5^{-/-}* or *Fundc1^{fl/y}Cdh5^{+/+}* mice and co-cultured the SVFs with CD31⁺ ATECs

isolated from either *Fundc1^{fl/y}Cdh5* (WT ATECs) or *Fundc1^{fl/y}Cdh5^{-/-}* (KO ATECs) mice. When co-cultured with WT ATEC, CD31⁺ SVFs from both *Fundc1^{fl/y}Cdh5* and *Fundc1^{fl/y}Cdh5^{-/-}* mice displayed comparable differentiation rates. However, when co-cultured with KO ATEC, CD31⁺ SVFs from both genotypes exhibited a significant reduction in lipid droplets formation (Supplementary Fig. 2f, g). Additionally, in the WT SVF, PA induced a significant reduction of insulin-induced 2-NBDG uptake by approximately 41.7%. However, in the KO SVF, this suppressive effect was mitigated, reducing the inhibition to around 27.8% (Fig. 1i). Taken together, these in vitro and ex vivo findings demonstrate that endothelial FUNDC1 is indispensable for adipocyte differentiation and the development of insulin resistance.

EC-specific deletion of *Fundc1* mice are protected from HFD-induced obesity&T2DM

Next, we treated *Fundc1^{fl/y}Cdh5* and *Fundc1^{fl/y}Cdh5^{-/-}* mice with either CD or HFD for 6 months. Body weight gains were comparable between the two groups under CD feeding, while HFD feeding induced greater weight gain in *Fundc1^{fl/y}Cdh5* mice compared to those on CD (Fig. 2a). However, *Fundc1^{fl/y}Cdh5^{-/-}* mice showed significantly less body weight gain relative to *Fundc1^{fl/y}Cdh5* mice under HFD feeding (Fig. 2a and Supplementary Fig. 3a). By the end of the experiment, deletion of endothelial FUNDC1 reduced HFD-induced body weight gain by 21.3% (Supplementary Fig. 3b). The anti-obesity effect of endothelial FUNDC1 deficiency was further supported by the observed reductions in fat percentage (reduced by 14.4% lower) and increases in lean percentage (17.5% higher) in *Fundc1^{fl/y}Cdh5^{-/-}* mice compared to *Fundc1^{fl/y}Cdh5* mice under HFD condition (Fig. 2b and Supplementary Fig. 3c).

We also assessed the effects of endothelial FUNDC1 on fat depots masses after chronic HFD consumption. Under CD feeding, the masses of epididymal white adipose tissue (EpiWAT), subcutaneous white adipose tissue (SubWAT), interscapular brown adipose tissue (BAT), and retroperitoneal white adipose tissue (RetWAT) were comparable between *Fundc1^{fl/y}Cdh5* and *Fundc1^{fl/y}Cdh5^{-/-}* mice (Fig. 2c). However, HFD significantly increased the masses of EpiWAT, SubWAT, and BAT in *Fundc1^{fl/y}Cdh5* mice, while these increases were attenuated in *Fundc1^{fl/y}Cdh5^{-/-}* mice, with reductions of 27% in SubWAT mass and 35% in BAT mass (Fig. 2c).

We further evaluated the morphology of adipose tissues. Under CD feeding, SubWAT adipocyte size was smaller in *Fundc1^{fl/y}Cdh5* mice compared to *Fundc1^{fl/y}Cdh5^{-/-}* mice (Fig. 2d-f). HFD feeding significantly increased adipocyte size in *Fundc1^{fl/y}Cdh5* mice, but this enlargement was mitigated in *Fundc1^{fl/y}Cdh5^{-/-}* mice, which also exhibited a marked increase in the frequency of smaller adipocytes. Taken together, these results suggest that endothelial FUNDC1 deletion confers protection against HFD-induced obesity.

EC-specific *Fundc1* deletion ameliorates HFD-induced diabetic metabolic disorders

To explore the effect of endothelial FUNDC1 on energy metabolism, we performed glucose tolerance test (GTT) and insulin tolerance test (ITT) in *Fundc1^{fl/y}Cdh5* and *Fundc1^{fl/y}Cdh5^{-/-}* mice. Under CD feeding, no significant differences in glucose tolerance or insulin resistance were observed between the two genotypes (Fig. 2g, h). However, under HFD conditions, *Fundc1^{fl/y}Cdh5^{-/-}* mice exhibited improved insulin sensitivity, as evidenced by a significantly enhanced glycemic profile in response to glucose or insulin administration and markedly reduced fasting glucose levels (Supplementary Fig. 3d). Notably, deletion of endothelial FUNDC1 did not alter serum insulin levels under either CD or HFD feeding conditions (Supplementary Fig. 3e). In addition, no differences in serum triglyceride (TG), total cholesterol (TC), or free fatty acid (FFA) levels were observed between the two genotypes under CD feeding (Supplementary Fig. 3f-h). However, under HFD conditions, *Fundc1^{fl/y}Cdh5^{-/-}* mice displayed significantly reduced serum FFA levels and increased Akt phosphorylation at Ser473 in SubWAT and BAT

(Supplementary Fig. 3i-k), suggesting enhanced insulin signaling in these tissues. These findings indicate that deletion of endothelial FUNDC1 may protect against HFD-induced diabetic phenotypes.

To elucidate the mechanisms underlying the resistance of *Fundc1^{fl/y}Cdh5^{-/-}* mice to HFD-induced obesity&T2DM, we measured the respiratory exchange ratio (RER) and energy expenditure using metabolic cages. HFD-fed *Fundc1^{fl/y}Cdh5* mice displayed a lower RER without changes in energy expenditure (Fig. 2i-l, black lines), suggesting reduced fat oxidation. In contrast, *Fundc1^{fl/y}Cdh5^{-/-}* mice showed a significantly restored RER coupled with increased energy expenditure under HFD conditions (Fig. 2i-l, red lines). Moreover, cumulative food intake (Supplementary Fig. 4a), water intake (Supplementary Fig. 4b), locomotor activity (Supplementary Fig. 4c), and cumulative distance (Supplementary Fig. 4d) were comparable between the two genotypes. These results demonstrate that *Fundc1^{fl/y}Cdh5^{-/-}* mice exhibit higher catabolic rates and preferentially utilize glucose as an energy source. Taken together, deletion of endothelial FUNDC1 attenuates HFD-induced metabolic disorders.

Deletion of endothelial FUNDC1 lessens HFD-induced vascular and endothelial dysfunction

Given that deletion of *Fundc1* prevents mitochondrial dysfunction in diabetic hearts, as previously reported^{20,21}, and that mitochondrial dysfunction is a central contributor to endothelial dysfunction in T2DM²⁶, we investigated whether EC-specific *Fundc1* deletion influences vascular function under obesity-induced T2DM. We first measured aortic stiffness in *Fundc1^{fl/y}Cdh5* and *Fundc1^{fl/y}Cdh5^{-/-}* mice using high-resolution ultrasound imaging. Under CD feeding, no significant differences in circumferential cyclic strain or pulse wave velocity were observed between the two genotypes (Supplementary Fig. 5a, b). However, HFD feeding significantly reduced circumferential cyclic strain and increased pulse wave velocity in carotid arteries of *Fundc1^{fl/y}Cdh5* mice, indicating pronounced arterial stiffness. In contrast, these impairments were mitigated in *Fundc1^{fl/y}Cdh5^{-/-}* mice, suggesting a protective role of endothelial FUNDC1 deletion against HFD-induced arterial stiffness.

Next, we evaluated acetylcholine (ACh)-mediated vasodilation in aortic rings from *Fundc1^{fl/y}Cdh5* and *Fundc1^{fl/y}Cdh5^{-/-}* mice. Under CD feeding, endothelial FUNDC1 deletion had no significant effect on either basal ACh-induced endothelium-dependent relaxation or sodium nitroprusside (SNP)-induced endothelium-independent vasodilation (Supplementary Fig. 5c-e). In contrast, HFD feeding impaired ACh-induced vessel relaxation in aortic rings from *Fundc1^{fl/y}Cdh5* mice, indicating endothelial dysfunction. However, this HFD-induced impairment in ACh-mediated relaxation was significantly alleviated in aortic rings from *Fundc1^{fl/y}Cdh5^{-/-}* mice (Supplementary Fig. 5c-e). These findings suggest that endothelial FUNDC1 deletion protects against HFD-induced endothelial dysfunction by preserving endothelium-dependent vasodilation.

We further investigated the impact of endothelial FUNDC1 deletion on vascular structure. Hematoxylin and eosin (H&E) staining of aortic sections showed no significant structural differences between genotypes under CD feeding conditions. However, HFD feeding significantly increased vascular wall thickness in *Fundc1^{fl/y}Cdh5* mice compared with CD-fed mice. In contrast, the vascular wall thickness was markedly reduced in HFD-fed *Fundc1^{fl/y}Cdh5^{-/-}* mice when compared to those in their littermates (Supplementary Fig. 5f, g). Additionally, HFD-fed *Fundc1^{fl/y}Cdh5* mice exhibited a significant increase in the collagen-to-elastic ratio, indicative of vascular remodeling. This increase was not observed in HFD-fed *Fundc1^{fl/y}Cdh5^{-/-}* mice (Supplementary Fig. 5f, h). Moreover, levels of 8-hydroxyguanosine (8-OHdG), a marker of oxidative DNA damage, were markedly elevated in the thoracic aortas, particularly in the EC layer, of HFD-fed *Fundc1^{fl/y}Cdh5* mice. However, endothelial FUNDC1 deletion significantly reduced the elevation of 8-OHdG levels

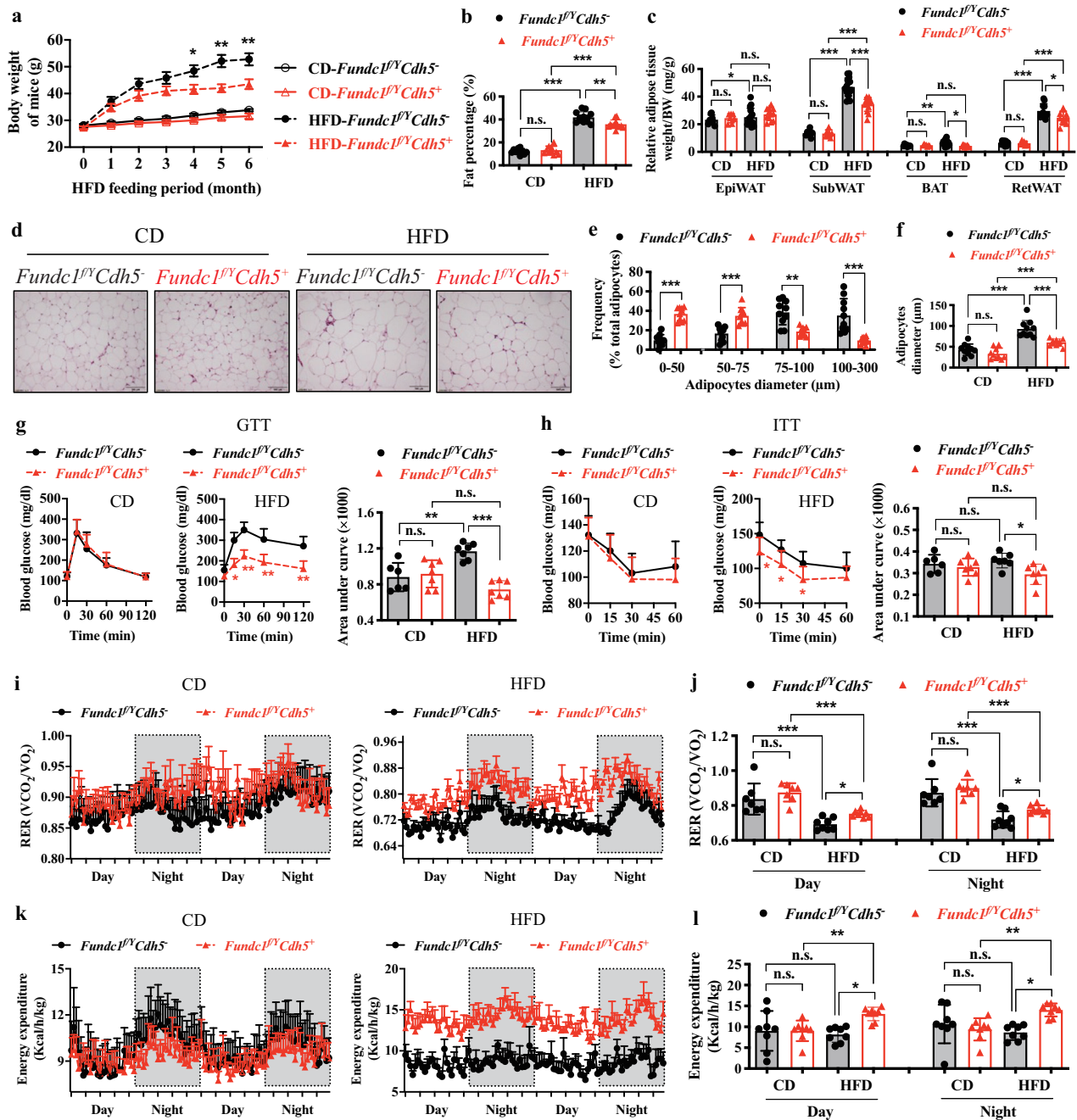


Fig. 2 | EC-specific *Fundc1* deletion mice exhibit resistance to HFD-induced obesity and metabolic dysfunction. **a–l** *Fundc1^{fl/y}* mice and littermates (*Fundc1^{fl/y}Cdh5^{-/-}*) were kept on HFD for 6 months. **a** Changes in body weight during HFD feeding. **p* < 0.05, ***p* < 0.01 (HFD-*Fundc1^{fl/y}Cdh5^{-/-}* vs. HFD-*Fundc1^{fl/y}*), *n* = 15–20. **b** Fat percentage of mice. *n* = 15–20 mice/group. **c** Adipose tissue weight/body weight. *n* = 15–20 mice/group. **d** Representative images of H&E staining of SubWAT. **e** Quantification of sizes and numbers of adipocytes under HFD feeding.

n = 15–20 mice/group. **f** Quantification of adipocyte diameter. *n* = 15–20 mice/group. **g** Glucose tolerance test (GTT) and quantification of the area under curve, *n* = 7–8 mice/group. **h** Insulin tolerance test (ITT) and quantification of the area under curve, *n* = 7–8 mice/group. **i, j** Whole body respiratory exchange ratio (RER; VCO_2/VO_2 , *n* = 8 mice/group). **k, l** Energy expenditure normalized to body weight, *n* = 8 mice/group. Data are presented as mean ± SD. * *p* < 0.05, ** *p* < 0.01, *** *p* < 0.001, n.s. *p* > 0.05.

(Supplementary Fig. 5i, j). In addition, we examined additional markers relevant to vascular functions. Specifically, we measured phosphorylated eNOS at Ser1177, phosphorylated VASP at Ser239 (a downstream marker of NO-cGMP signaling), and ET-B receptor (ETRB) expression in the aorta. None of these parameters showed significant differences between *Fundc1^{fl/y}Cdh5^{-/-}* and *Fundc1^{fl/y}* mice under normal conditions (Supplementary Fig. 6a–d). These findings demonstrate that endothelial *FUNDc1* deletion mitigates HFD-induced oxidative stress, vascular remodeling, and endothelial

dysfunction. Collectively, *Fundc1^{fl/y}Cdh5^{-/-}* mice exhibit resistance to HFD-induced vascular dysfunction.

Endothelial *FUNDc1* is required for HFD-induced angiogenesis and lipid-induced EC senescence in adipose tissues

To investigate the role of endothelial *FUNDc1* in adipose tissue development, we first examined the vascular density in subcutaneous white adipose tissue (SubWAT) using immunofluorescence staining in whole mount tissue. At 2 months of HFD feeding, CD31-positive

staining was significantly increased in *Fundc1^{fl/y}Cdh5* mice, indicative of enhanced angiogenesis (Supplementary Fig. 7a, b). In contrast, *Fundc1^{fl/y}Cdh5^{-/-}* mice exhibited markedly reduced CD31 signals under the same dietary condition, suggesting impaired angiogenic responses during early obesity.

To directly assess angiogenic capacity, we performed tube formation assays using MLECs. Compared to *Fundc1^{fl/y}Cdh5* controls, MLECs from *Fundc1^{fl/y}Cdh5^{-/-}* mice showed significantly diminished tube formation both under basal conditions and upon VEGF stimulation, which mimics early HFD-induced angiogenic cues (Supplementary Fig. 7c, d). Furthermore, long-term exposure to PA induced robust cellular senescence in MLECs from *Fundc1^{fl/y}Cdh5* mice, as evidenced by increased SA β -galactosidase staining. This PA-induced senescence was markedly attenuated in *FUND1*-deficient ECs (Supplementary Fig. 7e, f), suggesting a protective effect of *FUND1* loss against lipid-induced EC senescence. Taken together, these results indicate that endothelial *FUND1* is required for HFD-induced angiogenesis and contributes to EC susceptibility to lipotoxic stress.

Endothelial *FUND1* deletion suppresses the production of ET-1

Emerging evidence suggests that ECs are actively involved in maintaining metabolic homeostasis^{27,28}. To investigate the molecular mechanisms underlying the protective effects of endothelial *FUND1* deletion against HFD-induced obesity and vascular dysfunction, we screened for EC-secreted factors potentially associated with adipocyte metabolism. These included ET-1, transforming growth factor beta 1 (TGF- β 1), epidermal growth factor (EGF), fibroblast growth factor 2 (bFGF), hepatocyte growth factor (HGF), vascular endothelial growth factor (VEGF), bone morphogenetic protein 6 (BMP6), and platelet derived growth factor subunit (PDGF). Using Q-PCR analysis, we found that deletion of *Fundc1* specifically and significantly reduced ET-1 mRNA (*End1*) expression, while the expression levels of other factors, including *TGF- β 1*, *bFGF*, *HGF*, *VEGF*, *BMP6*, and *PDGF*, remained unaffected (Supplementary Fig. 8a). The reduction in *End1* expression due to EC-specific deletion of *Fundc1* was further confirmed by decreased ET-1 protein staining in the endothelium of *Fundc1^{fl/y}Cdh5^{-/-}* mice (Supplementary Fig. 8b, c). Consistently, silencing *FUND1* in human umbilical vein endothelial cells (HUVECs) also led to a significant reduction in ET-1 expression at both the protein and mRNA levels (Supplementary Fig. 8d-g).

Given the established role of ET-1 in the pathogenesis of obesity^{13,17,18,29}, we hypothesized that the protective effect of endothelial *FUND1* deletion against HFD-induced obesity is mediated through suppression of ET-1 production. To test this hypothesis, we assessed the impact of endothelial *FUND1* on ET-1 production during HFD feeding. As shown in Fig. 3a-c, plasma ET-1 levels in *Fundc1^{fl/y}Cdh5* mice were gradually upregulated, peaking at 6 weeks after HFD treatment and remaining elevated throughout the study period. In contrast, *Fundc1^{fl/y}Cdh5^{-/-}* mice exhibited significantly lower plasma ET-1 levels under HFD conditions, with levels remaining consistently lower than those in their *Fundc1^{fl/y}Cdh5* counterparts. Furthermore, endothelial *FUND1* deletion significantly reduced plasma ET-1 levels under both CD and HFD conditions (Fig. 3c). Notably, after 6 months of HFD feeding, deletion of endothelial *FUND1* reduced plasma ET-1 levels by 38% (Fig. 3b). Consistent with these findings, similar reductions in ET-1 mRNA levels were observed in the aortic intima of *Fundc1^{fl/y}Cdh5^{-/-}* mice (Fig. 3d).

ET-1 promotes insulin resistance in metabolic cells

To elucidate the role of ET-1 in obesity development, we examined its effects on the key processes involved in the expansion of WAT, including preadipocyte proliferation, migration, and differentiation. As shown in Fig. 3e-g, ET-1 stimulated 3T3-L1 preadipocyte migration and proliferation in a dose-dependent manner. Furthermore, when ET-1 was administered during the initial stages of 3T3-L1

differentiation, it significantly reduced adipocyte diameter while increasing intracellular triglyceride content compared to vehicle-treated controls (Supplementary Fig. 9a, b). In mature adipocytes, ET-1 promoted lipolysis, as evidenced by reduced intracellular lipid accumulation following treatment (Supplementary Fig. 9c, d). Q-PCR analysis revealed that ET-1 significantly upregulated the expression of lipolysis-related enzymes, including *ATGL*, *HSL*, *MGL*, and *Peri-A*, without altering the expression of adipocyte differentiation markers (*CEBP α* , *PPAR γ* , and *aP2 α*) or lipogenic transcription factors (*ACCI*, *FAS*, *SCD*, and *SREBP1c*) (Supplementary Fig. 9e). These findings collectively demonstrate that ET-1 enhances preadipocyte proliferation and promotes lipolysis in mature adipocytes, highlighting its role in adipose tissue expansion and remodeling.

Given the elevated ET-1 production observed in HFD-induced obesity, we hypothesized that ET-1 contributes to the development of insulin resistance in various metabolic organs, following increased lipolytic activity in adipose tissue. To investigate this, we examined the effects of ET-1 on insulin resistance in multiple metabolic cell types. In INS-1 832/16 β -cells, ET-1 treatment had no significant effect on glucose-stimulated insulin secretion (Fig. 3h). However, in primary islets isolated from C57BL/6J mice, ET-1 infusion significantly enhanced insulin secretion (Fig. 3i). In HepG2 hepatocytes and C2C12 myotubes, ET-1 treatment markedly exacerbated PA-induced lipid accumulation, as evidenced by Oil Red O staining and increased intracellular TG content (Fig. 3j, k). Given that ectopic fat accumulation in the liver and muscle is a key driver of insulin resistance, these findings collectively suggest that ET-1 promotes insulin resistance across multiple metabolic cell types.

ET-1 Infusion Blocks endothelial *FUND1* deletion-mediated attenuation of T2DM

To establish the role of ET-1 in ECs-specific *FUND1* deletion-mediated protection against HFD-induced T2DM and vascular dysfunction, *Fundc1^{fl/y}Cdh5^{-/-}* and *Fundc1^{fl/y}Cdh5* mice were infused with ET-1 (10 μ g/kg/day) for 4 weeks at the onset of a 5-month HFD treatment. After 4 weeks, ET-1 infusion increased plasma ET-1 levels by 1.86-fold in *Fundc1^{fl/y}Cdh5^{-/-}* mice and prevented the reduction of plasma ET-1 in *Fundc1^{fl/y}Cdh5* mice (Supplementary Fig. 10a). A similar trend was observed following 5 months of HFD feeding (Supplementary Fig. 10b). Consistent with previous findings, in the saline-treated groups, *Fundc1^{fl/y}Cdh5^{-/-}* mice exhibited significant reductions in body weight gain, fat mass (SubWAT and BAT), and fat percentage compared to their *Fundc1^{fl/y}Cdh5* littermates. However, in the ET-1 infusion groups, these differences were no longer observed, suggesting that ET-1 infusion negated the protective effects of endothelial *FUND1* deletion (Fig. 4a, b and Supplementary Fig. 10c, d). Notably, ET-1 infusion in *Fundc1^{fl/y}Cdh5^{-/-}* mice led to significant increases in body weight and SubWAT mass (Fig. 4a, b), though it did not affect fat and lean percentages (Supplementary Fig. 10c, d). Similarly, the metabolic benefits associated with endothelial *FUND1* deletion were abolished by ET-1 infusion, as indicated by comparable IPGTT and ITT curves and AUC values between *Fundc1^{fl/y}Cdh5^{-/-}* and *Fundc1^{fl/y}Cdh5* mice (Fig. 4c and Supplementary Fig. 10e, f), similar serum glucose (GLU), insulin, and FFA levels (Fig. 4d-f), no significant differences in metabolic cage-related parameters, including energy expenditure and activity levels (Supplementary Fig. 10g-n).

Furthermore, ET-1 infusion partially lowered the EC and vascular protective effects of *Fundc1* deletion, as shown by impaired EC function and increased arterial stiffness in *Fundc1^{fl/y}Cdh5^{-/-}* mice (Fig. 4g-k). These findings suggest that ET-1 infusion negates the protective effects of endothelial *FUND1* deletion against HFD-induced obesity and vascular dysfunction. Additionally, ET-1 serves as a key mediator linking endothelial dysfunction to metabolic dysfunction.

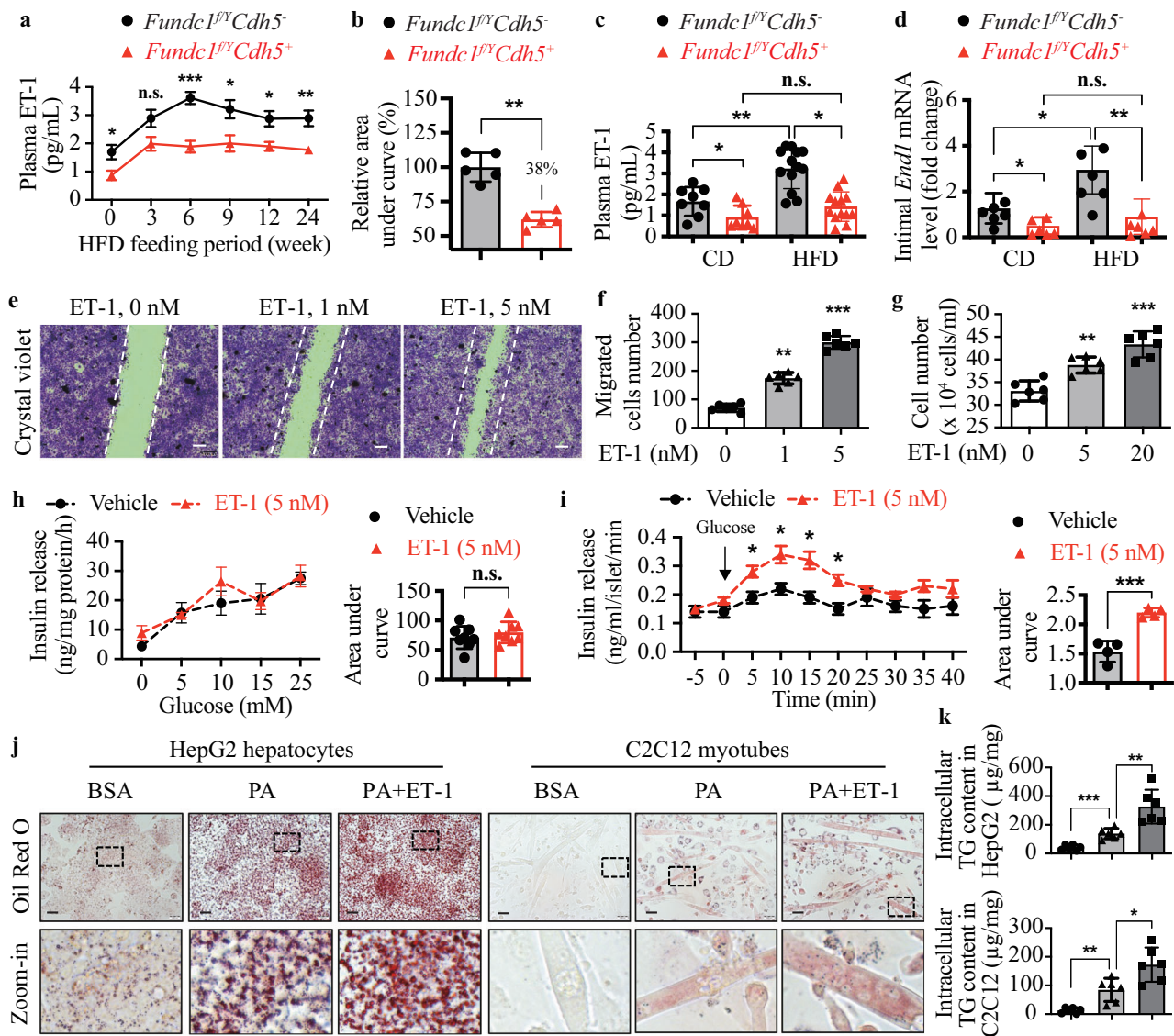


Fig. 3 | Endothelial FUNDC1 deletion suppresses the production of ET-1.

a Plasma ET-1 level in mice during HFD treatment, $n = 5$. **b** Quantification of the relative area under the curve of ET-1. $n = 5$ mice/group. **c** Plasma ET-1 level in mice after 6 months of HFD feeding, $n = 8-12$. **d** Q-PCR analysis of intimal ET-1 mRNA (*End1*) level. $n = 6$ mice/group. **e, f** Scratch assay of 3T3-L1 preadipocytes treated with indicated concentrations of ET-1 for 8 h and quantification of the migrated cell number, scale bar: 50 μm . $n = 6$ independent experiments. **g** Cell numbers of 3T3-L1 pre-adipocytes treated with indicated concentrations of ET-1 for 24 h, $n = 6$

independent experiments. **h** Glucose-induced insulin release in INS-1832/16 β -Cells. $n = 8$ independent experiments. **i** Glucose-induced insulin release in primary islets from C57BL/6J mice. $n = 4$ mice/group. **j** Representative images of HepG2 hepatocytes and C2C12 myotubes treated with or without 5 nM ET-1 in the present of 200 μM PA for 48 h. Cells treated with BSA were set as control group, scale bar: 50 μm . **k** Quantification of intracellular TG contents in **j**. $n = 6$ independent experiments. Data are presented as mean \pm SD, * $p < 0.05$, ** $p < 0.01$, *** $p < 0.001$, n.s. $p > 0.05$.

Lack of FUNDC1 downregulates GATA2 to inhibit ET-1 production

To investigate the mechanism by which FUNDC1 regulates ET-1 production, we transfected HUVECs with either control siRNA (siCtrl) or FUNDC1 siRNA (siFUNDC1) and examined the expression of key proteins involved in the proteolytic processing of ET-1 precursors and its transcriptional regulation. Specifically, we analyzed endothelin-converting enzyme 1 (ECE1), which processes ET-1 precursors into biologically active ET-1, as well as key transcription factors regulating ET-1 expression, including GATA-binding protein 2 (GATA2) and activator protein 1 (AP-1/c-JUN). As shown in Fig. 5a, b, *FUNDC1* knockdown significantly reduced GATA2 protein levels but did not affect ECE1 or AP-1 protein expression. Additionally, *FUNDC1* silencing did not alter the mRNA expression of *ECE1*, *GATA2*, or *c-JUN* (Fig. 5c). Conversely, *FUNDC1* overexpression enhanced GATA2 protein expression but had no effect on ECE1 or AP-1

protein levels (Fig. 5d, e). To determine whether GATA2 directly regulates ET-1 production, we assessed *EDN1* mRNA levels following *GATA2* silencing. As shown in Fig. 5f, *GATA2* deficiency significantly reduced *EDN1* mRNA expression. Interestingly, along with the decreased FUNDC1 protein levels, the expression of both GATA2 and ET-1 increased in response to PA stimulation under normal conditions. However, in FUNDC1-deficient cells, this elevation of GATA2 and ET-1 was completely abolished (Fig. 5g-j). Collectively, these findings suggest that ECs-specific FUNDC1 deletion downregulates GATA2 protein expression, thereby inhibiting *EDN1* transcription and reducing ET-1 production.

FUNDC1 deficiency reduces GATA2 protein level by promoting SIRT3-L translocation from mitochondria to the nucleus

We further investigated the mechanism by which FUNDC1, a mitochondrial outer membrane protein, regulates GATA2, a protein

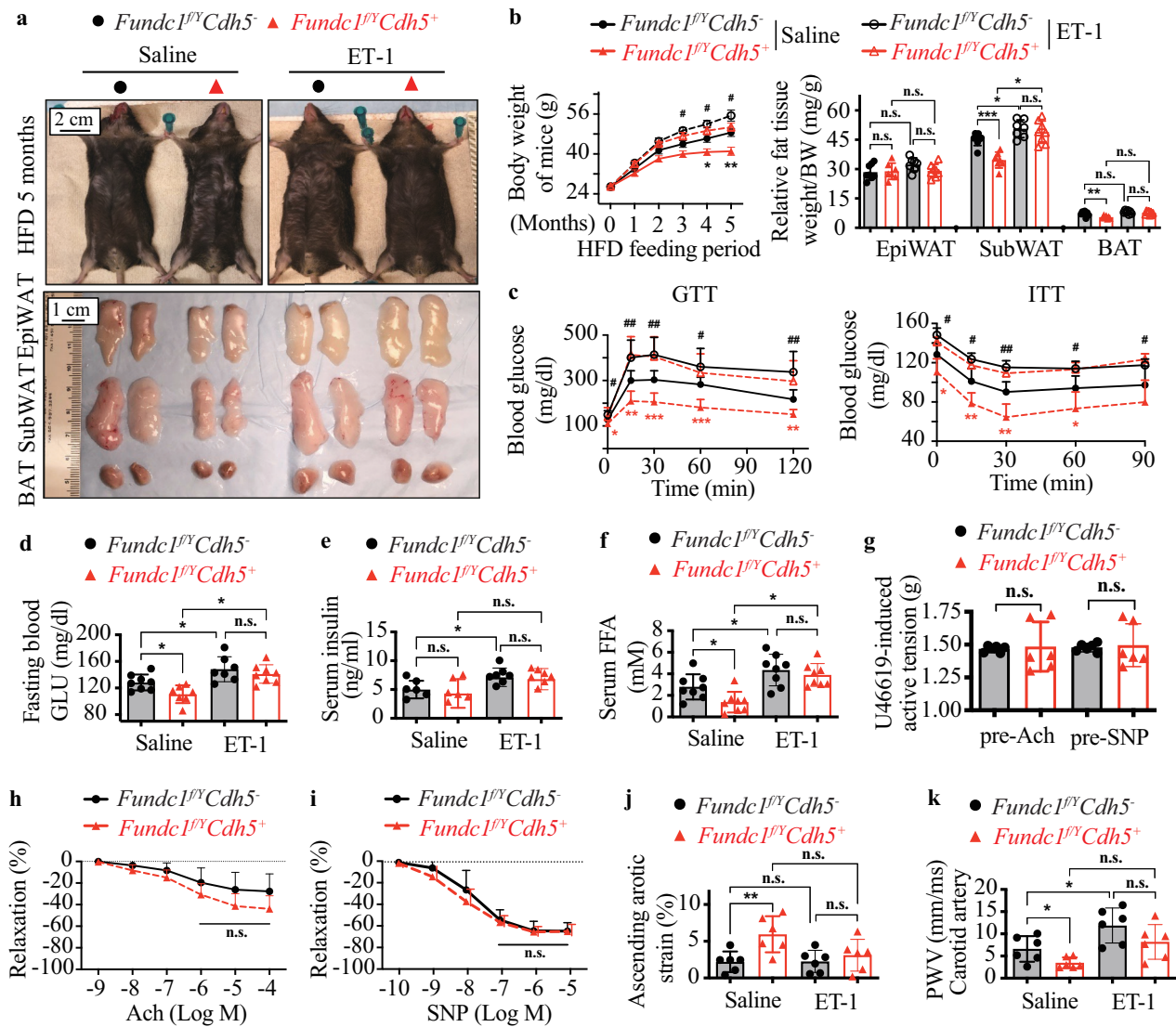


Fig. 4 | ET-1 infusion at early-stage reverses endothelial FUNDC1 deletion-mediated anti-obesity and vascular protective effects. Mice were placed on a high-fat diet (HFD) and infused with ET-1 (10 µg/kg/day) or saline concurrently, starting at the onset of HFD feeding, using subcutaneously implanted osmotic pumps for 4 weeks. **a** Representative pictures of whole body, epididymal white adipose tissue (EpiWAT), subcutaneous white adipose tissue (SubWAT), and brown adipose tissue (BAT). **b** Changes in body weight during HFD feeding periods (left panel), * $p < 0.05$, ** $p < 0.01$ (Saline-*Fundc1^{fl/y}Cdh5* vs. Saline-*Fundc1^{fl/y}Cdh5⁺*), #

$p < 0.05$, ## $p < 0.01$ (ET-1-*Fundc1^{fl/y}Cdh5* vs. ET-1-*Fundc1^{fl/y}Cdh5⁺*), and relative weights of adipose tissues (right panel). $n = 7-8$ mice/group. **c** Glucose tolerance test (IPGTT) and insulin tolerance test (ITT). $n = 7-8$ mice/group. **d** Fasting blood glucose (GLU) level. $n = 7-8$ mice/group. **e** Serum insulin level. $n = 7-8$ mice/group. **f** Serum free fatty acid (FFA) level. $n = 7-8$ mice/group. **g-i** Aortic ring vasoreactivity assay in ET-1-infused mice. $n = 6$ mice/group. **j, k** Circumferential cyclic strain (**j**) and (PWV) pulse wave velocity (**k**) of carotid artery. $n = 6$ mice/group. Data are presented as mean \pm SD. * $p < 0.05$, ** $p < 0.01$, *** $p < 0.001$, n.s. $p > 0.05$.

predominantly localized in the nucleus^{30,31}. Mitochondria are known to sense stress signals and transmit them to the nucleus to initiate adaptive responses, a process that often involves the redistribution of nuclear or mitochondrial proteins between the two compartments³². Sirtuin 3 (SIRT3) was initially thought to be exclusively localized in mitochondria, but recent studies have demonstrated its presence in the nucleus as well^{33,34}. Notably, SIRT3 deficiency has been shown to accelerate HFD-induced obesity and endothelial dysfunction in mice^{35,36}. Given this, we examined whether SIRT3 plays a role in regulating GATA2 expression. As shown in Fig. 6a-c, transfection of SIRT3 siRNA (siSIRT3) significantly reduced the protein levels of both the long (SIRT3-L) and short (SIRT3-S) isoforms. This was accompanied by a marked increase in GATA2 protein levels, without affecting GATA2 mRNA expression. Consequently, *EDNI* mRNA expression was significantly upregulated. Conversely, *SIRT3* overexpression markedly decreased GATA2 protein levels (Supplementary Fig. 11a, b), indicating

that SIRT3 negatively regulates GATA2 expression at the post-transcriptional level.

To investigate how FUNDC1 regulates GATA2 via SIRT3, we first examined whether FUNDC1 affects SIRT3 protein expression. We found that neither *FUNDC1* silencing nor *FUNDC1* overexpression altered total SIRT3 protein levels, including both the long (SIRT3-L) and short (SIRT3-S) isoforms (Supplementary Fig. 11c-f). Next, we assessed whether SIRT3 physically interacts with FUNDC1 and GATA2. HUVEC lysates were immunoprecipitated with an anti-SIRT3 antibody and subsequently immunoblotted with anti-FUNDC1 or anti-GATA2 antibodies. As shown in Fig. 6d, both FUNDC1 and GATA2 were detected in the SIRT3-immunoprecipitated samples, indicating endogenous interactions. Furthermore, immunofluorescence staining revealed that FUNDC1 is localized in mitochondria, GATA2 is primarily found in the nucleus, and SIRT3 is present in both mitochondria and the nucleus. Co-localization analysis confirmed that SIRT3 interacts

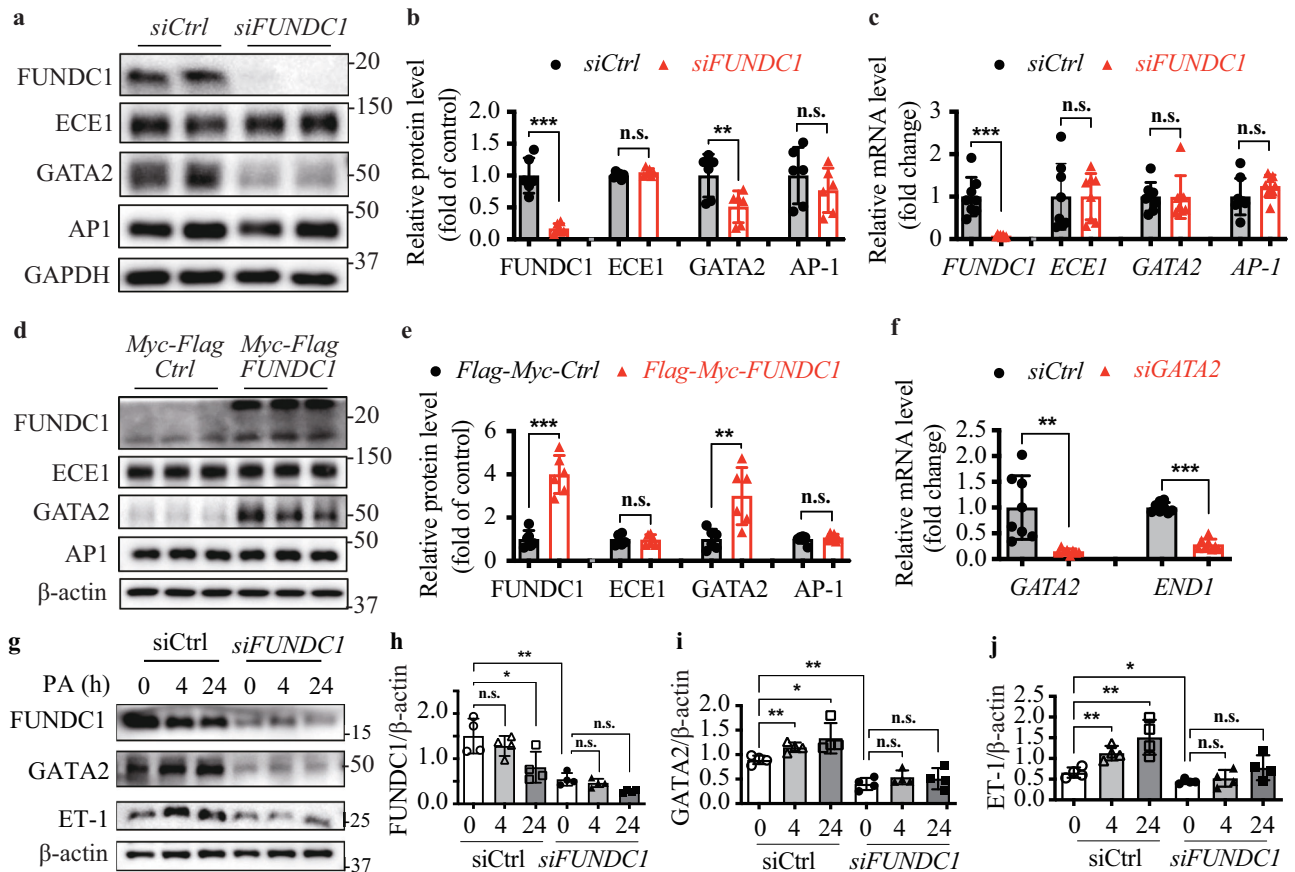


Fig. 5 | Lack of *FUNDC1* downregulates GATA2 to inhibit ET-1 production.

a HUVECs were transfected with control siRNA (siCtrl) or *FUNDC1* siRNA (siFUNDC1) and subjected to immunoblotting analysis. **b** Quantification of protein levels of ECE1, GATA2, and AP1. **c** HUVECs were transfected with control siRNA (siCtrl) or *FUNDC1* siRNA (siFUNDC1) and subjected to Q-PCR analysis to detect ECE1, AP1, and *JUN* mRNA levels. **d** HUVECs were transfected with control Myc-Flag-tagged plasmid (Myc-Flag-Ctrl) or Myc-Flag-FUNDC1 plasmid (Myc-Flag-FUNDC1) and subjected to immunoblotting

analysis. **e** Quantification of protein levels of FUNDC1, ECE1, GATA2 and AP1 in (d). $n = 6$ independent experiments. **f** HUVECs were transfected with control siRNA (siCtrl) or *GATA2* siRNA (siGATA2) and subjected to Q-PCR analysis to detect *EDN1* mRNA levels. $n = 8$ independent experiments. **g** HUVECs were transfected with control siRNA (siCtrl) or *FUNDC1* siRNA (siFUNDC1) and were then treated with 200 μ M PA for indicated time periods. **h-j** Quantification of protein levels of FUNDC1, GATA2, and ET-1 in (g). $n = 4$ independent experiments. Data are presented as mean \pm SD, * $p < 0.05$, ** $p < 0.01$, *** $p < 0.001$, n.s. $p > 0.05$.

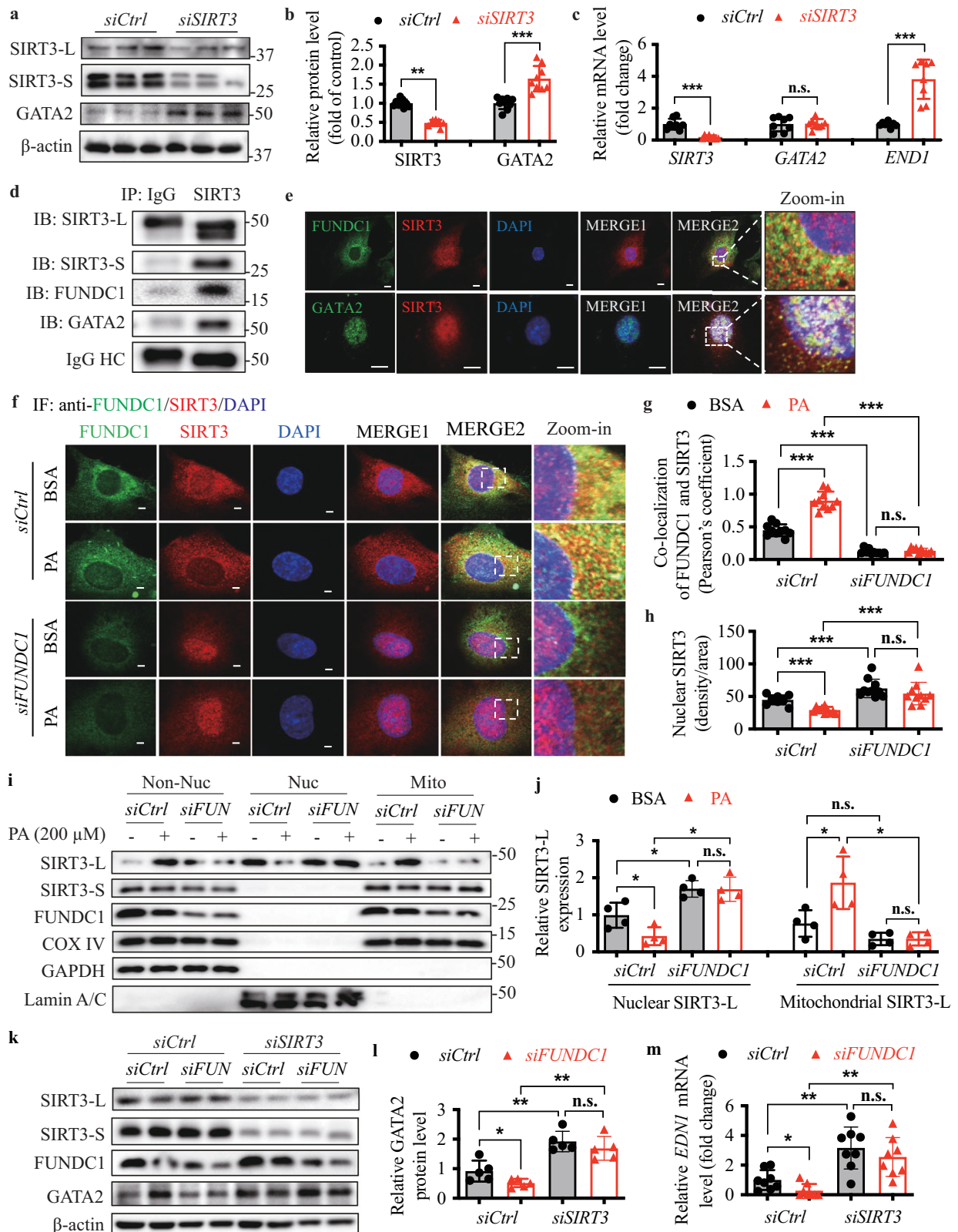
with FUNDC1 in mitochondria and with GATA2 in the nucleus (Fig. 6e), supporting the notion that SIRT3 can physically associate with both FUNDC1 and GATA2.

We next investigated whether *FUNDC1* deficiency affects the subcellular distribution of SIRT3 in HUVECs treated with PA. In control siRNA-transfected cells, PA treatment promoted the translocation of SIRT3 from the nucleus to mitochondria, as indicated by increased colocalization of SIRT3 with FUNDC1 and reduced nuclear SIRT3 density (Fig. 6f, g). However, in *FUNDC1*-deficient cells, SIRT3 remained localized in the nucleus under both BSA- and PA-treated conditions (Fig. 6f-h). These findings were further validated by western blot analysis of SIRT3 protein levels in subcellular fractions (Fig. 6i, j). The results confirmed that SIRT3-L is expressed in both the nucleus and mitochondria, whereas SIRT3-S is exclusively localized in mitochondria, and that PA treatment reduced nuclear SIRT3-L levels while increasing mitochondrial SIRT3-L in control cells. *FUNDC1* silencing led to increased nuclear SIRT3-L and decreased mitochondrial SIRT3-L in BSA-treated cells, a redistribution that was partially blocked under PA-treated conditions, indicating that SIRT3-L translocated from mitochondria to the nucleus in *FUNDC1*-deficient cells. Finally, we tested whether SIRT3 is involved in the regulation of GATA2 and ET-1 expression in *FUNDC1*-deficient conditions by knocking down both *SIRT3* and *FUNDC1* in HUVECs. As shown in Fig. 6k-m, *SIRT3* silencing increased GATA2 protein and *EDN1* mRNA expression, and prevented

the *FUNDC1*-deficiency-induced reduction of GATA2 protein and *EDN1* mRNA expression. Taken together, these findings suggest that *FUNDC1* deficiency blocks PA-induced translocation of SIRT3-L from the nucleus to mitochondria, leading to sustained nuclear SIRT3-L retention, which suppresses GATA2-mediated ET-1 production.

FUNDC1 deficiency enhances GATA2 degradation via promoting SIRT3-mediated GATA2 deacetylation

Since *SIRT3* silencing increased GATA2 protein levels without affecting its mRNA expression, we hypothesized that SIRT3 plays a role in GATA2 protein stability. To test this, HUVECs were transfected with control siRNA (siCtrl) or *SIRT3* siRNA (siSIRT3), followed by treatment with cycloheximide (CHX) to inhibit protein synthesis. GATA2 protein decay was then assessed over a 240 min period. In control cells, GATA2 protein levels gradually declined, with an estimated half-life of 60 min. After 240 min of CHX treatment, GATA2 protein levels had decreased by 75.3%. However, in *SIRT3*-deficient cells, GATA2 degradation was markedly attenuated. The half-life of GATA2 extended beyond 4 hours, and GATA2 protein levels remained stable even after 6 h of CHX treatment, indicating that *SIRT3* silencing enhances GATA2 stability (Fig. 7a, b). Given that SIRT3 is a sirtuin deacetylase, and GATA2 is an acetylated protein, with lysine acetylation known to regulate protein stability and function³⁷⁻³⁹, we investigated whether SIRT3 affects GATA2 acetylation. Immunoprecipitation and western blot analysis



revealed that *SIRT3* silencing significantly increased GATA2 acetylation (Fig. 7c, d). Additionally, PA treatment reduced SIRT3 expression, which was accompanied by enhanced GATA2 acetylation (Fig. 7e, f). Together, these findings suggest that SIRT3 promotes GATA2 degradation by reducing its acetylation, thereby regulating GATA2 protein stability. Additionally, FUNDC1 was found to be negatively regulated by SIRT3, as evidenced by the increased FUNDC1 protein levels (but

not mRNA levels) under SIRT3-silencing conditions, while its levels decreased upon SIRT3 overexpression (Fig. 7g-k). Moreover, FUNDC1 protein stability, evaluated by CHX treatment, was enhanced in SIRT3-deficient conditions (Fig. 7l, m). Therefore, these data suggest that SIRT3 regulates FUNDC1 protein stability. Importantly, to assess whether the patterns observed in HUVECs are recapitulated in vivo, we examined the expression of GATA2 and SIRT3-L in ECs from HFD-fed

Fig. 6 | *FUNDC1* deficiency suppresses *GATA2* protein level by promoting *SIRT3-L* translocation from mitochondria to the nucleus. **a** HUVECs were transfected with control siRNA (siCtrl) or *SIRT3* siRNA (*siSIRT3*) and subjected to immunoblotting analysis. **b** Quantification of protein levels in (a). $n = 8$ – 10 independent experiments. **c** HUVECs were transfected with control siRNA (siCtrl) or *SIRT3* siRNA (*siSIRT3*) and subjected to Q-PCR analysis to detect mRNA levels of *GATA2* and *END1*. $n = 8$ independent experiments. **d** The interactions between *SIRT3* and *FUNDC1* or *GATA2* in HUVECs were determined by immunoprecipitation (IP) and immunoblotting (IB) analysis. **e** The co-localization of *SIRT3* and *FUNDC1* or *GATA2* were determined by immunofluorescence staining. Nuclei were stained by DAPI. MERGE1 indicates merge of *SIRT3* and DAPI; MERGE2 indicates merge of *FUNDC1*, *SIRT3*, and DAPI; MERGE3 indicates merge of *GATA2* and DAPI; MERGE4 indicates merge of *GATA2*, *SIRT3*, and DAPI. Scale bar: $10 \mu\text{m}$. **f** HUVECs were transfected with control siRNA (siCtrl) or *FUNDC1* siRNA (*siFUNDC1*) in the presence of BSA or $200 \mu\text{M}$ PA and subjected to immunofluorescence staining analysis. MERGE1 indicates merge of *SIRT3* and DAPI; MERGE2 indicates merge of *FUNDC1*, *SIRT3*, and

DAPI. Scale bar: $10 \mu\text{m}$. **g** Pearson's coefficient calculated by ZEN software, indicates the co-localization of *FUNDC1* and *SIRT3*. $n = 9$ cells from three independent experiments. **h** Quantification of nuclear *SIRT3* level. **i** HUVECs were transfected with control siRNA (siCtrl) or *FUNDC1* siRNA (*siFUN*) in the presence of BSA or $200 \mu\text{M}$ PA. Non-nuclear fraction (Non-Nuc), nuclear fraction (Nuc), and mitochondria fraction (Mito) were prepared and subjected to immunoblotting analysis. $n = 9$ cells from three independent experiments. **j** Quantification of protein level of *SIRT3* long isoform (*SIRT3-L*) in the nucleus (Nuclear *SIRT3-L*) and in mitochondria (Mitochondrial *SIRT3-L*). $n = 4$ independent experiments. **k** HUVECs were double transfected with control siRNA (siCtrl) or *FUNDC1* (*siFUN*) and *SIRT3* siRNA and subjected to immunoblotting analysis. **l** Quantification of *GATA2* protein level in (k). $n = 5$ independent experiments. **m** HUVECs were double transfected with either control siRNA (siCtrl) or *FUNDC1* and *SIRT3* siRNA and subjected to Q-PCR analysis to detect *END1* mRNA level. $n = 8$ independent experiments. Data are presented as mean \pm SD, * $p < 0.05$, ** $p < 0.01$, *** $p < 0.001$, n.s. $p > 0.05$.

Fundc1^{fl/y}Cdh5^{Cre+} mice and controls. Consistent with our in vitro findings, *GATA2* expression was elevated under nutrient-excess conditions but markedly suppressed upon *FUNDC1* deletion (Supplementary Fig. 12a–d). These results demonstrate that the *FUNDC1/SIRT3-L/GATA2* regulatory axis identified in HUVECs is also active in mouse endothelium during metabolic stress, thereby reinforcing the physiological relevance of our proposed mechanism.

FUNDC1-mediated *SIRT3-L* translocation is potentially associated with HSC70 chaperone system

A recent study demonstrated that *FUNDC1* can directly interact with the chaperone HSC70 to coordinate mitochondrial proteostatic stress responses⁴⁰, to further delineate the mechanistic basis of the *FUNDC1-SIRT3-L* interaction, we investigated whether the HSC70 chaperone system contributes to this process. Sequence analysis revealed that both *FUNDC1* and *SIRT3* harbor potential KFERQ-like motifs (Fig. 8a), suggesting their capacity to interact with HSC70. Indeed, IP assays and IF staining confirmed that both *FUNDC1* and *SIRT3-L* associate with HSC70 in HUVECs (Fig. 8b, c). Consistently, knockdown of HSC70 markedly diminished the binding between *FUNDC1* and *SIRT3-L*, as shown by reduced co-immunoprecipitation efficiency (Fig. 8d–f) These findings were further substantiated by subcellular fractionation and immunoblotting of *SIRT3* isoforms (Fig. 8g, h). Silencing HSC70 resulted in nuclear accumulation and reduced mitochondrial localization of *SIRT3-L* under basal conditions, a redistribution that was partially attenuated under PA stimulation. Together, these results indicate that HSC70 may facilitate *FUNDC1*-dependent mitochondrial recruitment of *SIRT3-L*, and that loss of HSC70 impairs this process, thereby promoting nuclear retention of *SIRT3-L*.

Upregulation of *FUNDC1/GATA2/ET-1* signaling in human patients with obesity&T2DM

To further investigate the relevance of *FUNDC1* regulation of endothelial ET-1 to human obesity and T2DM, we measured plasma ET-1 levels in age-matched healthy donors ($n = 17$) and donors with both obesity and T2DM ($n = 19$; see Fig. 9a for patient characteristics). As shown in Fig. 9b, plasma ET-1 levels were significantly higher in the obesity and T2DM group compared to healthy individuals. Moreover, plasma ET-1 levels were positively correlated with BMI ($p < 0.0001$, Fig. 9c) and HbA1c levels ($p < 0.05$, Fig. 9d). Next, we assessed *FUNDC1*, *END1*, and *GATA2* mRNA levels in intima isolated from small arterioles. Compared to healthy individuals, donors with obesity and T2DM exhibited significantly higher mRNA levels of *FUNDC1*, *END1*, and *GATA2* in the intima (Fig. 9e). Furthermore, intimal *END1* mRNA levels correlated positively with *FUNDC1* ($p < 0.0001$, Fig. 9f) and *GATA2* ($p < 0.0001$, Fig. 9g). Notably, intimal *FUNDC1* mRNA levels also showed a strong positive correlation with plasma ET-1 levels ($p < 0.01$, Fig. 9h). Similarly, protein levels of *FUNDC1*, ET-1, and *GATA2* were

significantly elevated in whole small arterioles from patients with obese and T2DM compared to healthy donors (Fig. 9i, j). Additionally, immunostaining revealed markedly increased expression of *FUNDC1* and ET-1 in the endothelium of femoral arteries from patients with obese and T2DM (Fig. 9k, l). Taken together, these findings suggest that an *FUNDC1/GATA2/ET-1* regulatory pathway is present in human arteries and is more active under obesity and T2DM conditions.

Discussion

Our findings reveal that ECs-specific *Fundc1* deletion mice are protected from obesity-induced T2DM. Mechanically, overnutrition-induced stress promotes the translocation of *SIRT3-L* from the nucleus to mitochondria, where *FUNDC1* functions as a key mitochondrial receptor for this translocation. Loss of *FUNDC1* disrupts *SIRT3-L* mitochondrial relocation, leading to its retention in the nucleus, where it promotes *GATA2* degradation by reducing its acetylation. Since *GATA2* is a transcriptional regulator of ET-1, a potent driver of insulin resistance, *FUNDC1* deletion suppresses ET-1 production. Moreover, *SIRT3* negatively regulates *FUNDC1* expression, suggesting a feedback mechanism (Fig. 10). In human diabetic patients, both *FUNDC1* ET-1 levels are elevated compared to healthy donors, further supporting a link between *FUNDC1* and ET-1 regulation.

Our study highlights the critical role of *FUNDC1* as a mitochondrial receptor for *SIRT3-L* translocation, which is essential for regulating nuclear *GATA2* activity and ET-1 production. The loss of *FUNDC1* leads to nuclear retention of *SIRT3-L*, impairing its function in promoting *GATA2* degradation and thereby suppressing ET-1 expression. Given the established role of ET-1 in insulin resistance and T2DM, *FUNDC1* may act as a key modulator of metabolic homeostasis. Intriguingly, *SIRT3* also negatively regulates *FUNDC1*, suggesting a complex regulatory network. Furthermore, our findings suggest that endothelial *FUNDC1* plays a stage-dependent role in the progression from obesity to type 2 diabetes. In the early phase of obesity, *FUNDC1* facilitates angiogenesis, which is consistent with our previous finding that deficiency of endothelial *FUNDC1* inhibits angiogenesis by decreasing mitochondria-associated endoplasmic reticulum membranes formation⁴¹, likely supporting adipose tissue expansion by providing sufficient vascular capacity and nutrient supply⁴². However, under chronic metabolic stress, such as prolonged lipid overload, endothelial *FUNDC1* appears to contribute to EC senescence, a pathological change that may underlie impaired insulin signaling and vascular dysfunction. Mechanistically, this dual role of *FUNDC1* may be mediated, at least in part, by its regulation of ET-1 production. Given that ET-1 promotes both angiogenesis and insulin resistance, *FUNDC1*-driven ET-1 expression could represent a molecular switch linking adaptive vascular remodeling to metabolic deterioration. These insights

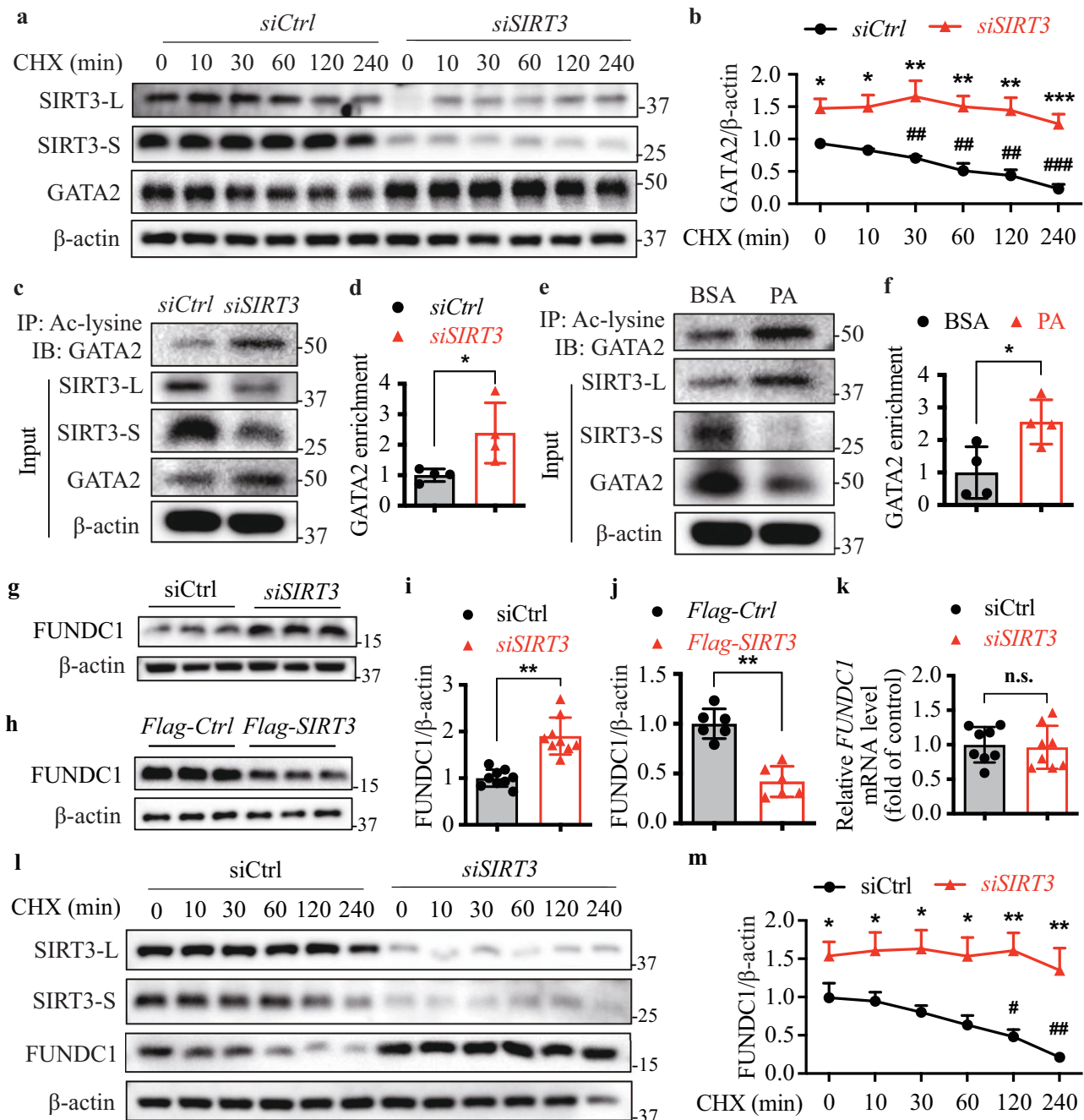


Fig. 7 | Deacetylation of GATA2 by SIRT3 promotes GATA2 degradation in FUNDC1-deficient conditions. **a** HUVECs were transfected with control siRNA (siCtrl) or *SIRT3* siRNA and then treated with 50 μ g/ml cycloheximide (CHX) for 240 min. Cell lysates were subjected to immunoblotting analysis. **b** Quantification of GATA2 protein level in (a). $n = 4$ independent experiments. **c** Acetylated GATA2 level was determined by IP of acetylate lysine (Ac-lysine) in cells transfected with *SIRT3* siRNA and followed by immunoblotting (IB) of GATA2. **d** Quantification of the enrichment of acetylated GATA2 in (c). $n = 4$ independent experiments. **e** Acetylated GATA2 level was determined by IP of Ac-lysine in cells treated with PA (200 μ M) and followed by immunoblotting (IB) GATA2. **f** Quantification of the enrichment of acetylated GATA2 in (e). $n = 4$ independent experiments. **g** HUVECs were transfected with control siRNA (siCtrl) or *SIRT3* siRNA (siSIRT3) and subjected to immunoblotting analysis. **h** HUVECs were transfected with control Myc-Flag-

tagged plasmid (*Myc-Flag-Ctrl*) or *Myc-Flag-SIRT3* plasmid (*Myc-Flag-SIRT3*) and subjected to immunoblotting analysis. **i, j** Quantification of protein levels of FUNDC1. $n = 6-9$ independent experiments. **k** HUVECs were transfected with control siRNA (siCtrl) or *SIRT3* siRNA (siSIRT3) and subjected to Q-PCR analysis to detect *FUNDC1* mRNA level. $n = 8$. **l** HUVECs were transfected with control siRNA (siCtrl) or *SIRT3* siRNA and then treated with 50 μ g/ml cycloheximide (CHX) for 240 min. Cell lysates were subjected to immunoblotting analysis. **m** Quantification of GATA2 protein level in (l). $n = 3$ independent experiments. Data are presented as mean \pm SD, in (b and m), star represents the comparison between groups siCtrl and siSIRT3 at the same treatment intervals, pound represents the comparison with control group (time = 0 min). * $p < 0.05$, ** $p < 0.01$, *** $p < 0.001$, n.s. $p > 0.05$. # $p < 0.05$, ## $p < 0.01$, ### $p < 0.001$, n.s. $p > 0.05$.

position FUNDC1 as a critical modulator of EC function that orchestrates the transition from nutrient-induced vascular activation to dysfunction, thereby contributing to the sequential development of obesity and T2DM.

In our study, endothelial-specific *Fundc1* deletion resulted in approximately 27% less body weight gain under HFD feeding, a magnitude that likely represents a major driver of the improved metabolic phenotype. Given the well-established relationship between adiposity

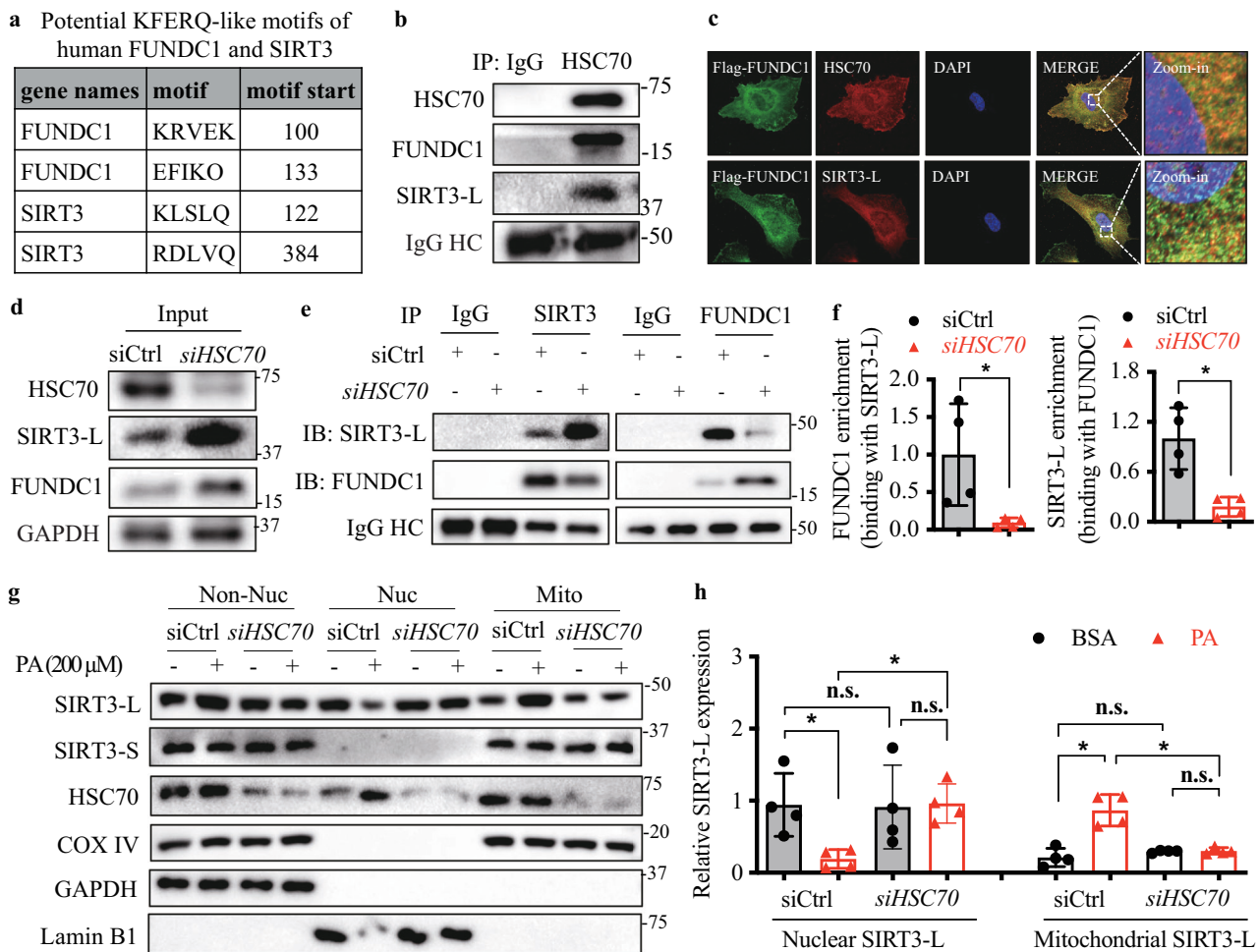


Fig. 8 | FUNDC1-mediated SIRT3-L translocation is potentially associated with HSC70 chaperone system. **a** Potential KFERQ-like motifs of human FUNDC1 and SIRT3. **b** Interactions between HSC70 with FUNDC1 and SIRT3-L in HUVECs were detected by IP and IB. **c** Co-staining of FUNDC1 with HSC70 and SIRT3-L by IF. **d** Interaction of SIRT3-L and FUNDC1 was analyzed in HUVECs transfected with HSC70 siRNA. **e** Quantification of protein levels in HUVECs transfected with HSC70 siRNA. **f** Quantification of the binding activity of FUNDC1 with SIRT3-L in HSC70 knockdown cells, indicated by the enrichment of FUNDC1. *n* = 4 independent

experiments. **g** HUVECs were transfected with control siRNA (siCtrl) or HSC70 siRNA (siHSC70) in the presence of BSA or 200 μM PA. Non-nuclear fraction (Non-Nuc), nuclear fraction (Nuc), and mitochondria fraction (Mito) were prepared and subjected to immunoblotting analysis. **h** Quantification of protein level of SIRT3 long isoform (SIRT3-L) in the nucleus (Nuclear SIRT3-L) and in mitochondria (Mitochondrial SIRT3-L). *n* = 4 independent experiments. Data are presented as mean ± SD. * *p* < 0.05, ** *p* < 0.01 derived from Student's *t* tests.

and vascular dysfunction, this reduction in weight gain is expected to contribute substantially to the preserved endothelial function and enhanced insulin sensitivity observed in *Fundc1^{fl/y}Cdh5⁺* mice. Nevertheless, several endothelial-intrinsic alterations were detected directly in isolated ECs, including reduced ET-1 expression, diminished adipose angiogenic capacity, and altered SIRT3-L/GATA2 signaling. While these changes may participate locally in shaping endothelial behavior, their contribution relative to the dominant systemic effect of reduced adiposity remains uncertain.

ET-1, beyond its role as an endothelium-derived vasoconstrictor, plays a critical part in adipose tissue metabolism and development, positioning it as a key driver in the progression from obesity to T2DM. Elevated ET-1 activity is closely linked to overweight and obesity^{29,43,44}, with chronic ET-1 infusion promoting adipocyte hyperplasia by activating the protein kinase C pathway through the ET A receptor¹². This process enhances pre-adipocyte proliferation while suppressing adipocyte differentiation, contributing to dysfunctional adipose tissue expansion. ET-1 administration has been shown to induce whole-body insulin resistance in both rodents and humans, potentially through the acceleration of lipolysis^{13,45-47}, which increases circulating FFA levels

and exacerbates lipotoxicity⁴⁸⁻⁵⁰. In our study, ET-1 infusion at 10 μg/kg/day, a dose previously reported not to affect blood pressure under normal diet conditions⁵¹, led to significant endothelial dysfunction, and adipocyte hyperplasia under HFD conditions. These findings underscore the pivotal role of ET-1 in linking endothelial dysfunction with obesity-driven metabolic deterioration. By driving adipose tissue expansion and promoting insulin resistance, ET-1 serves as a crucial mediator in the transition from obesity to T2DM, highlighting its potential as a therapeutic target for metabolic disease intervention.

An important aspect of our study is that a 4-week ET-1 infusion, administered only during the initial phase of HFD feeding, was sufficient to restore adipocyte hyperplasia and long-term weight gain in *Fundc1^{fl/y}Cdh5⁺* mice. Although exogenous ET-1 exposure was “transient”, this period overlaps with a critical window of adipose tissue plasticity during early HFD feeding, when endothelial-adipocyte communication exerts disproportionate and durable effects on tissue architecture and metabolic set-points. Thus, even short-term perturbations in ET-1 signaling may produce lasting consequences for adipose expansion and metabolic trajectory. Integrating established principles from ET-1 biology, adipose tissue remodeling, and

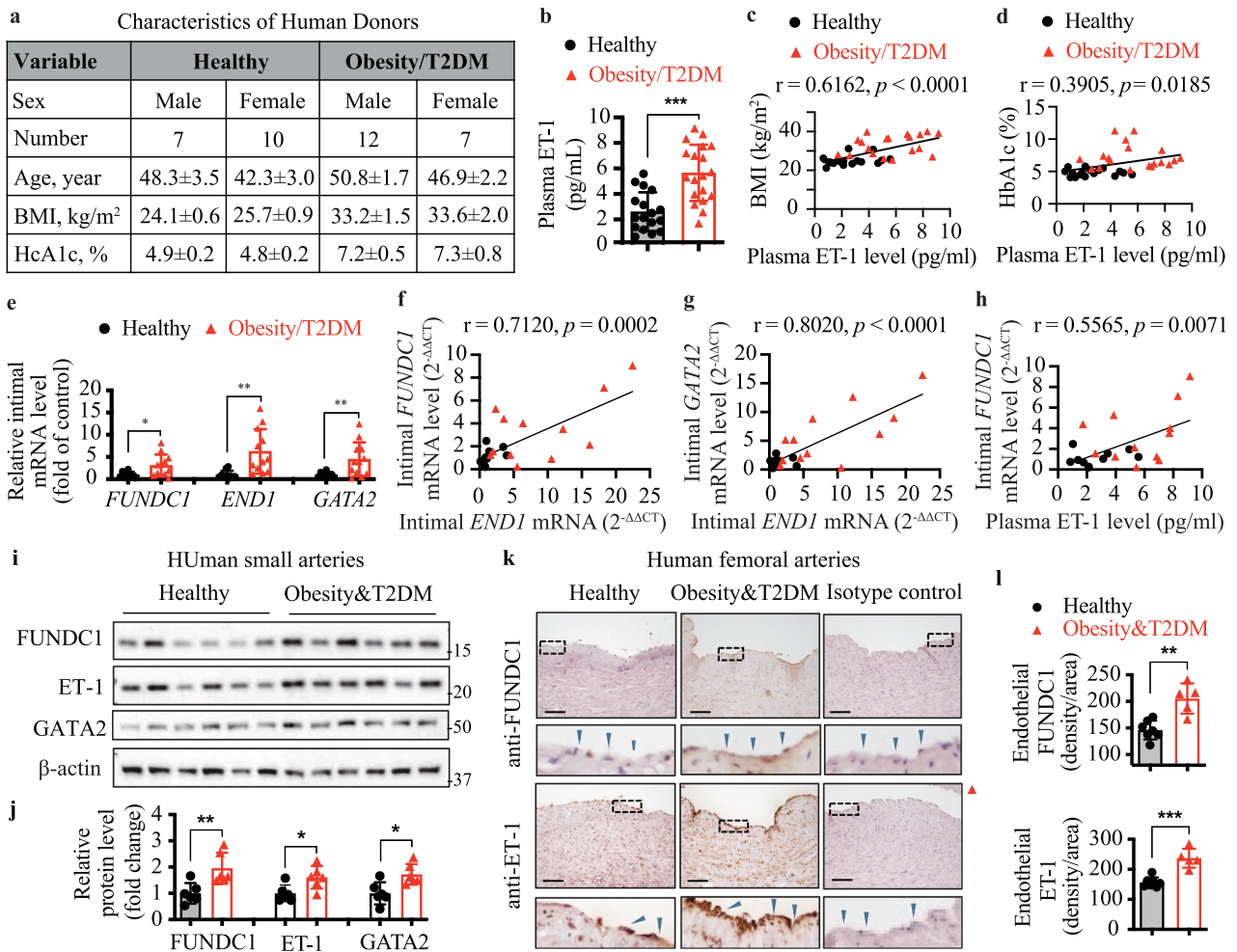


Fig. 9 | Upregulation of FUNDC1/GATA2/ET-1 signaling in human patients with diabetic obesity. Plasma and endothelium were collected from age-matched healthy donors ($n = 17$) or donors with both obesity and T2DM (Obesity&T2DM, $n = 19$). **a** Characteristics of human donors. Age, body mass index (BMI), and glycohemoglobin A1c (HbA1c) levels are represented as mean \pm SD. **b** Plasma ET-1 level in human donors. $n = 17$ –19 donors/group. **c** Spearman’s correlation of plasma ET-1 level and BMI. **d** Spearman’s correlation of plasma ET-1 level and HbA1c. **e** qPCR analysis of *FUNDC1*, *END1* and *GATA2* mRNA levels in the intima isolated from human small arterioles. $n = 17$ –19 donors/group. **f** Spearman’s correlation of mRNA

levels of *FUNDC1* and *END1*. **g** Spearman’s correlation of mRNA levels of *GATA2* and *END1*. **h** Spearman’s correlation of intimal *FUNDC1* mRNA and plasma ET-1. **i, j** Human small arterioles were collected from age-matched healthy donors or donors with both obesity and T2DM (Obesity&T2DM) and subjected to western blot analysis (**i** and **j**). $n = 6$ donors/group. **k, l** Human femoral arteries were collected from age-matched healthy donors ($n = 7$) or donors with both obesity and T2DM (Obesity&T2DM; $n = 5$) and subjected to IHC staining. Scale bar: 50 μ m. Data are presented as mean \pm SD. * $p < 0.05$, ** $p < 0.01$, *** $p < 0.001$, n.s. $p > 0.05$.

endothelial-stromal crosstalk, we propose that early ET-1 elevation may initiate a series of processes with persistent impact: (1) expansion of the adipocyte progenitor pool, enabling sustained hyperplasia; (2) induction and stabilization of microvascular networks that persist after ET-1 withdrawal and facilitate continued adipose growth; (3) epigenetic reprogramming of endothelial or stromal lineages that shifts transcriptional programs toward a growth-permissive state; (4) recruitment of macrophages that establish a chronic inflammatory niche; (5) extracellular matrix remodeling that imposes durable structural changes; (6) early adipocyte hyperplasia, which permanently increases total adipocyte number; and (7) feed-forward activation of endogenous ET-1 pathways that may continue beyond the cessation of exogenous ET-1 delivery. Collectively, these potential mechanisms provide a biologically coherent framework explaining how short-term ET-1 elevation during early HFD feeding can set a long-term trajectory of adipose expansion and thereby restore the obese phenotype in *Fundc1^{fl/y}Cdh5⁺* mice.

In addition to its metabolic consequences, endothelial FUNDC1 deletion appeared to influence vascular function. ECs are central

regulators of vascular homeostasis, and ET-1 is a well-established mediator of vasoconstriction, inflammation, and vascular remodeling during metabolic stress. In our model, *Fundc1^{fl/y}Cdh5⁺* mice exhibited reduced ET-1 expression and showed modest improvement in endothelial relaxation. These changes, however, occurred alongside substantial reductions in body weight, a key factor known to markedly improve vascular function. For this reason, the vascular phenotype observed in *Fundc1^{fl/y}Cdh5⁺* mice is likely driven primarily by their attenuated obesity, with reduced ET-1 signaling contributing but may not acting independently. ET-1 infusion in HFD-fed mice further impaired endothelial function, supporting the relevance of ET-1 in vascular dysregulation, but the available data do not allow us to separate endothelial-intrinsic effects from systemic metabolic influences. Overall, endothelial FUNDC1 may participate in ET-1-related endothelial responses, but in the context of HFD feeding, reduced adiposity appears to be the dominant determinant of vascular outcomes in *Fundc1^{fl/y}Cdh5⁺* mice.

SIRT3 is a NAD⁺-dependent mitochondrial deacetylase that regulates acetylation levels in mitochondria, which is essential for many

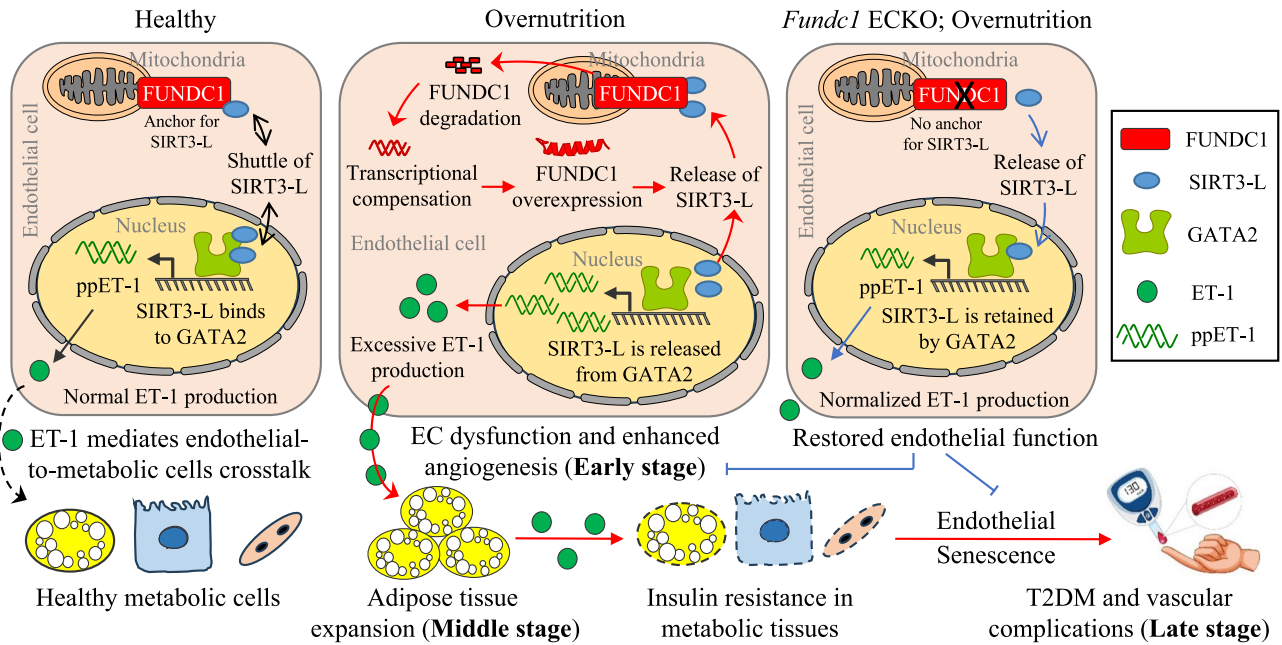


Fig. 10 | Schematic description that endothelial FUNDC1 regulates the progression from obesity to T2DM. In the healthy state, endothelial FUNDC1 anchors SIRT3-L in mitochondria, limiting its nuclear accumulation and regulating its interaction with GATA2, thereby maintaining normal ET-1 production and preserving vascular and metabolic homeostasis. Under overnutrition-induced metabolic stress, SIRT3-L is released from GATA2, contributing to enhanced GATA2-mediated ET-1 transcription. Elevated ET-1 promote angiogenesis to provide the space for adipocyte hyperplasia at the early stage and later exacerbate insulin resistance and thus driving the progression from obesity to T2DM. Importantly, SIRT3-L translocation to mitochondria also facilitates FUNDC1 degradation at the early obese

stage, which triggers a compensatory increase in FUNDC1 transcription and ultimately results in FUNDC1 overexpression in a late-stage. The elevation of FUNDC1 further enhances mitochondrial recruitment of SIRT3-L, amplifying ET-1 production. In contrast, in *Fundc1* EC-specific knockout (ECKO) mice, the absence of FUNDC1 prevents mitochondrial recruitment of SIRT3-L, leading to its nuclear retention, where SIRT3-L promotes GATA2 degradation and suppresses ET-1 transcription. The loss of *Fundc1* in ECs not only suppresses angiogenesis at early overnutrition stage but also prevents EC senescence at late stage to attenuate the potential diabetic vascular complications.

cellular processes, including energy metabolism, oxidative stress, mitochondrial biogenesis, and cell survival⁵². SIRT3 is also a stress-responsive protein that can transport between mitochondria and the nucleus upon cellular stress^{33,53}. Previous studies show that SIRT3 can be induced by energetic stress, caloric restriction, H₂O₂, etoposide, and UV-irradiation, we further identify PA as a novel stimulus to regulate SIRT3 subcellular distribution. PA treatment has no effect on SIRT3 protein expression but promotes the long isoform of SIRT3 translocation from the nucleus to mitochondria. Under FUNDC1-sufficient conditions, FUNDC1 recruits and attaches SIRT3-L in mitochondria. However, when lacking FUNDC1, SIRT3-L remains in the nucleus and interacts with GATA2, reducing its lysine acetylation and stability, thus leading to suppressed ET-1 transcripts. These findings expand the current understanding of both FUNDC1 and SIRT3 by highlighting functions that are mechanistically distinct from their canonical roles. FUNDC1 has traditionally been studied as a regulator of mitochondrial quality control, notably through its role in mitophagy, mitochondrial fission, ER-mitochondria contact, and calcium homeostasis^{21–23,54}. Similarly, SIRT3 is well known for its mitochondrial deacetylase activity in controlling oxidative metabolism and EC glycolysis^{55,56}. Our results reveal that FUNDC1 also governs the nuclear-mitochondrial shuttling of SIRT3-L, linking mitochondrial dynamics to nuclear transcriptional regulation. Through this FUNDC1/SIRT3-L/GATA2 signaling axis, ECs integrate metabolic stress signals with transcriptional control of ET-1, thereby establishing a novel mechanism by which mitochondrial proteins influence vascular and metabolic homeostasis.

An intriguing observation in our study was that 2 months of HFD feeding did not induce statistically significant insulin resistance (Fig. 1), a finding that contrasts with reports of much earlier glucose intolerance. The onset of dysglycemia following HFD is known to be

highly variable and influenced by multiple experimental factors, including diet composition and energy density, mouse strain or substrain, age at diet initiation, housing conditions, microbiota, and the protocols used for glucose and insulin tolerance testing. While some studies report impairments in glucose tolerance within just a few days of HFD exposure⁵⁷, others describe preserved glucose tolerance for several weeks⁵⁸. These discrepancies support the notion that short- and long-term HFD exposure may involve distinct pathogenic mechanisms, with ectopic lipid accumulation driving early alterations and chronic inflammation exerting a stronger influence at later stages. Such dynamics may lead to fluctuations in both the timing and magnitude of insulin resistance. Notably, vascular responses to lipid challenge arise very rapidly and are often detectable well before persistent systemic insulin resistance develops. Indeed, a recent systematic review and meta-analysis demonstrated that even a single high-fat meal can transiently impair EC function, reflected by reduced flow-mediated dilation, within hours of ingestion⁵⁹. Collectively, these findings reinforce our interpretation that endothelial dysfunction represents an early and sensitive marker of nutritional excess.

Despite the strengths of our study, several limitations should be acknowledged. First, although we report an intriguing discrepancy between FUNDC1 mRNA and protein expression under different metabolic stress conditions, the precise post-transcriptional mechanisms underlying this divergence remain undefined. A recent study suggest that PA can promote the shift of FUNDC1 from its dimeric to monomeric form via enhanced production of lysophosphatidylinositol, leading to increased acetylation at lysine K104⁶⁰. This acetylated monomeric FUNDC1 is subsequently targeted by MARCH5 for proteasomal degradation. These mechanistic insights may partially explain the early decline of FUNDC1 protein

observed in our models, even in the presence of stable or elevated mRNA levels, while further investigation is needed to determine whether similar regulatory mechanisms operate in vivo under chronic metabolic stress. We also acknowledge the apparent discrepancy between elevated GATA2 mRNA levels in obese patients and the reduced GATA2 protein stability observed upon FUNDC1 knockdown in vitro. This difference likely reflects distinct layers of regulation: chronic metabolic stress may transcriptionally upregulate GATA2 in human endothelium, whereas enhanced FUNDC1 turnover under lipotoxic conditions through PA-induced acetylation and MARCH5-mediated ubiquitination may attenuate its suppressive effect on GATA2 protein stability. Thus, increased mRNA but reduced protein turnover may coexist, underscoring the importance of both transcriptional and post-translational mechanisms in regulating GATA2 during obesity. Second, while our human data show that both FUNDC1 mRNA and protein levels are elevated in endothelium from obese individuals with T2DM, this observation lacks a metabolically healthy obese control group, and our current human data are based on a relatively small cohort and do not yet establish direct mechanistic causality. This limitation precludes us from determining whether increased FUNDC1 expression is a general feature of obesity or a specific hallmark of disease progression toward T2DM. As such, the causal role of endothelial FUNDC1 in the transition from obesity to diabetes in humans remains to be fully clarified. Stratified clinical studies including non-diabetic obese individuals will be necessary to validate our proposed model of FUNDC1-mediated endothelial dysfunction and ET-1 overproduction in the pathogenesis of metabolic disease. Another limitation is that we could not directly confirm whether GATA2 and SIRT3-L mediate the vascular and metabolic phenotypes in *Fundc1^{fl/y}Cdh5⁺* mice. As functional delivery of recombinant proteins of GATA2 or SIRT3-L is limited by their poor cell permeability, and EC-specific genetic models are technically challenging due to embryonic lethality and systemic effects, future studies using advanced genetic or targeted delivery approaches are needed to clarify their causal roles in FUNDC1-dependent endothelial dysfunction and metabolic deterioration.

Collectively, our findings demonstrate that ET-1 levels are elevated in the endothelium of obese and diabetic individuals, positioning it as a key mediator in the transition from obesity to T2DM. The deletion of endothelial FUNDC1, which inhibits ET-1 production, provides significant protection against obesity-induced metabolic dysfunction and vascular impairment in HFD-fed mice. Our study establishes ET-1 as a crucial inter-organ signaling molecule that facilitates communication between ECs and metabolic tissues to regulate systemic metabolic homeostasis. Moreover, the regulation of FUNDC1 and suppression of ET-1 emerge as promising therapeutic strategies to mitigate adipose tissue dysfunction, vascular abnormalities, and metabolic disorders associated with obesity and T2DM.

Methods

Human specimens

Human blood and tissue (small arterioles, including mesenteric artery and superficial femoral artery) samples were obtained from patients undergoing bariatric surgery or diabetic amputations or donors undergoing gastrectomy or amputation surgery for traffic accident. Obesity was defined as a body mass index (BMI) of ≥ 30.0 , and type 2 diabetes mellitus (T2DM) was identified as the percentage of glycated hemoglobin A1c (HbA1c) of $\geq 6.5\%$ or based on diagnosis in the donors' medical records. All procedures involving human specimens complied with the principles outlined in the 1975 Declaration of Helsinki and were approved by the Ethics Committee of Chu Hsien-I Memorial Hospital of Tianjin Medical University (NO. ZXYJNYKMEC2023-38). Informed consent was obtained from each participating patient prior to the procedure.

Animal procedure

The *Fundc1* gene is located in chromosome X²¹. The floxed-*Fundc1* mice were developed by the Mouse Biology Program (University of California, Davis). The constitutive *Cre^{Cdh5+}* mice were purchased from the Jackson Laboratory (Bar Harbor, ME). The EC-specific *Fundc1* knockout (*Fundc1^{fl/y}Cdh5⁺*) mice were generated by crossing female *Fundc1^{fl/y}Cdh5^{+/+}* with male *Fundc1^{fl/y}Cdh5^{+/+}* mice. Littermate *Fundc1^{fl/y}Cdh5^{-/-}* mice were considered as control mice. All mice in C57BL/6J background were maintained on a 12:12 h light-dark cycle at $21 \pm 2^\circ\text{C}$ and were given free access to water and food. The diet-induced obesity model was produced by feeding 10-week-old male *Fundc1^{fl/y}Cdh5^{-/-}* and *Fundc1^{fl/y}Cdh5^{+/+}* mice on an HFD (20% protein, 35% carbohydrate, 45% fat, total 5.7 kcal/g, D12451, Research Diet, New Brunswick, NJ) or a chow diet (20% protein, 70% carbohydrate, 10% fat, D12450B, Research Diet, New Brunswick, NJ) for 6 months. The animal protocol in this study (A25012) was approved by the Institutional Animal Care and Use Committee at Georgia State University. An expanded Materials and Methods section is available in the Methods in the Data Supplement.

Body composition

Body weight was measured and recorded monthly. Body composition was assessed by nuclear magnetic resonance technology (Bruker Minispec; Billerica, MA) and the fat and lean percentages were calculated.

Glucose and insulin tolerance tests

Glucose and insulin tolerance tests were performed as described previously with slight modification⁶¹. Briefly, the mice were fasted for 16 h for the glucose tolerance test (GTT) and 6 h for insulin tolerance test (ITT). After examination of the baseline fasting blood glucose level, each animal received glucose (Sigma-Aldrich, G7528) at a dosage of 1.5 g/kg body weight or insulin (Sigma-Aldrich, I9278) at a dosage of 0.5 U/kg body weight, via intraperitoneal injection. Blood glucose levels were determined using glucometer at 15, 30, 60, and 120 min after glucose injection for GTT, or at 15, 30, and 60 min after insulin injection for ITT. Serum insulin concentrations were measured using ELISA kit (ALPCO, 80-INSMS-E01; Salem, NH). Serum free fatty acid level was determined using EnzyChrom™ Free Fatty Acid Assay Kit (BioAssay Systems, EFA-100). Serum contents of triglyceride and total cholesterol were measured using Infinity kit (Thermo Fisher Scientific, TR22421, TR13421; Waltham, MA).

Indirect calorimetry analysis

The metabolic rate of mice was measured using calorimetric systems (PhenoMaster, TSE Systems, Bad Homburg, Germany). Mice were housed individually with *ad libitum* access to food and water and acclimatized to respiratory chambers for 3 days before the experiments. The data for O₂ consumption (VO₂), CO₂ production (VCO₂), calorie (food and water) intake and locomotor activity were recorded in real time for 3–5 days. Respiratory exchange ratio (RER) and energy expenditure were determined using LabMaster software. The RER was calculated as the ratio of VCO₂ to VO₂ and energy expenditure (kcal/kg/h) was calculated with the following formula: $(3.815 \times \text{VO}_2 + 1.232 \times \text{VCO}_2)/1000$.

Measurements of aortic stiffness

Vascular ultrasound was performed using a Vevo 3100 Imaging System (FUJIFILM VisualSonics, Toronto, ON, Canada) as described previously⁶². Briefly, under 2% isoflurane anesthesia, the mouse carotid artery was first visualized in B mode on the transverse plane, and then the transducer was switched to obtain images on the longitudinal plane. Anterior and posterior aortic wall motion was assessed using images captured in M mode. Images were finally analyzed using the Vevo WorkStation. Systolic diameter (Ds) and diastolic diameter (Dd) were quantified from M-mode images, and circumferential cyclic strain

was then calculated with the following formula: (Ds-Dd)/Dd. The aortic pulse wave velocity (PWV) was calculated as the distance traveled by the pulse wave divided by the time taken to travel the distance.

Vascular reactivity measurements

Vessel reactivity was analyzed by organ chamber (Radnoti LLC, Monrovia, CA), as described previously⁶³. Mouse descending aortic rings were pre-contracted with 30 nM U46619 (Cayman, 16450). At the plateau of contraction, endothelium-dependent responses were determined in the presence of acetylcholine (ACh; Sigma-Aldrich, A6625) at concentrations of 10^{-9} to 10^{-4} M, and endothelium-independent vasodilation was determined in the presence of Sodium Nitroprusside (SNP; Sigma-Aldrich, 567538) at concentrations of 10^{-10} to 10^{-5} M.

Plasma ET-1 determination and infusion of ET-1 in mice

Plasma ET-1 peptide concentration was determined by an enzyme-linked immunosorbent assay (ELISA) kit (R&D Systems, DET100; Minneapolis, MN) according to the manufacturer's instruction. Plasma was obtained from the blood collected by orbital puncture. Aliquots of plasma (200 μ l) were immediately treated with ice-cold 3,4-dichloroisocoumarin solution (148 μ g/ml) immediately, and rapidly vortexed to prevent conversion of big ET-1 to ET-1 during sample processing⁶⁴. Assay was conducted immediately after sample collection or aliquot and store samples at -80°C , avoiding repeated freeze-thaw cycles.

Subcutaneous infusion of ET-1. Male *Fundc1^{fl/y}Cdh1^{fl/y}* and *Fundc1^{fl/y}Cdh1^{fl/y}* mice were subcutaneously implanted an Alzet osmotic minipump (Alzet, model 1004, Cupertino, CA) filled with either sterile saline (0.9% NaCl) or ET-1 (Enzo, ALX-155-001-P001) at a dosage of 10 μ g/kg/day (in sterile saline), a dose that does not significantly enhance blood pressure⁶⁵. All mice were fed an HFD or CD immediately after the implantation. After 28-day infusion of ET-1, the minipumps were removed, and the mice were kept feeding on their respective diets for another 4 months.

Cell culture and primary cell isolation

HUVECs were obtained from American Type Culture Collection (ATCC, PCS-100-013; Manassas, VA) and maintained in Eagle's Basal Medium (EBM; Lonza, CC-3121; Walkersville, MD) supplemented with 5% (v/v) fetal bovine serum (FBS; Sigma-Aldrich, F0926, St Louis, MO), growth factors (Lonza, CC-4133), and 1% (v/v) antibiotics penicillin and streptomycin (Gibco, 15140-122; Grand Island, NY). When the cells were grown to 70–80% confluence, the medium was switched to the culture medium containing 2% FBS. HUVECs at passages 3 to 8 were used in the experiments.

Mouse 3T3-L1 pre-adipocytes were purchased from ATCC (CL-173) and cultured in Dulbecco's modified Eagle's medium (DMEM, Corning, 10-017-CV; Herndon, Virginia) containing 10% (v/v) FBS and 1% (v/v) antibiotics penicillin and streptomycin. The medium was routinely changed every 2–3 days until the cells reached a confluent state. Differentiation was induced by culturing the cells in DMEM supplemented with 0.5 mM 3-isobutyl-1-methylxanthine (IBMX; Sigma-Aldrich, I7018), 1 μ M dexamethasone (Sigma-Aldrich, D4902), and 1.5 μ g/ml insulin (Sigma-Aldrich, I6634). Adipocytes were used 8–10 days after differentiation, when 90–95% of the cells exhibited adipocyte phenotype. All cells were incubated in a humidified atmosphere of 5% CO₂ and 95% air at 37 $^{\circ}\text{C}$. 3T3-L1 pre-adipocytes at passages 5–10 were used in the experiments.

Isolation of primary MLECs was performed as described previously⁶⁶. Briefly, lung tissue was excised, minced, digested with collagenase type I (Worthington, LS004196), triturated with a 30-cc syringe, and passed through a 70 μ m cell strainer. Anti-CD31-coated beads (BD Bioscience, 553369) were added to the cell suspension, mixed, and incubated for 10 min at room temperature. The bead-bound cells were isolated with a magnet, resuspended in EBM containing 20% (v/v) FBS, ECs growth factor, and 1% (v/v) antibiotics, and

plated on Fibronectin-coated cell culture dish. When approached confluence, the cells were detached, suspended, and incubated with anti-CD102-coated Dynabeads (BD Biosciences, 553325). The bead-bound cells were isolated with a magnet, resuspended in EBM containing 20% (v/v) FBS, ECs growth factor, and 1% (v/v) antibiotics and plated in Fibronectin-coated cell culture dish.

Isolation of ATEC were performed as previously described. Briefly, subcutaneous fat was collected, minced, and incubated in Krebs Ringer HEPES buffer (29.2 g/mol NaCl, 42.0 g/mol NaHCO₃, 37.25 g/mol KCl, 68.05 g/mol KH₂PO₄, 73.5 g/mol CaCl₂, 123.25 g/mol MgSO₄, and 20 mM HEPES) containing 1% BSA and 1 mg/mL collagenase type I under shaking (100 rpm) at 37 $^{\circ}\text{C}$ for 30 min. The ratio of fat weight to digest solution was 1:4. The resultant digested material was filtered through a sterile 300 μ m cell strainer (pluriSelect, 43-50300-50) to remove larger aggregates. Adipocytes and free oil were separated from the stromal vascular fractions (SVF) by centrifugation at 1500 rpm for 6 min. The resulting pellet (i.e., the SVF) was resuspended and plated onto 1% gelatin-coated cell culture dish in ECs growth medium (as above) containing 10% FBS. To select ATECs, the mixed cell suspension was cultured for 3–5 days. Next, the cells were collected and incubated with anti-CD31-coated Dynabeads for 15 min at 4 $^{\circ}\text{C}$. The selected cells were plated onto 1% gelatin-coated cell culture dish in ECs growth medium (as above) containing 10% FBS. When cells grew to confluence, the cells were further purified by anti-CD102-coated Dynabeads.

Cell treatments

Palmitic acid (PA) was prepared by conjugating with fatty-acid-free bovine serum albumin (BSA). To evaluate the long-term effect of PA on FUNDC1 expression in HUVECs, cells were incubated with 200 μ M PA conjugated to fatty acid-free BSA, and culture medium containing PA or BSA was refreshed daily throughout the 7-day stimulation period to maintain a consistent lipid challenge. To study the effect of ET-1 on proliferative activity of 3T3-L1 preadipocytes, 3T3-L1 cells without differentiation were treated with ET-1 (5 and 20 nM) for 24 h, followed by trypan blue cell counting test using an automated cell counter (Bio-rad, TC20).

Scratch wound healing assay was performed to study the effect of ET-1 on 3T3-L1 preadipocytes migration. After 3T3-L1 preadipocytes had nearly formed a confluent cell monolayer, a linear wound was gently made in the monolayer using a sterile 200- μ l pipette tip. The distance of the gap was recorded at the starting time point and the cells were treated with either ET-1 (1 and 5 nM) or vehicle (0.9% NaCl) for 8 h. Repeated observations of the edge of the same scratched lesion were performed. Images were captured using a microscope (IX71, Olympus) equipped with a digital camera and the migrated cells number were calculated.

To study the effect of initiative effect of ET-1 on adipocytes differentiation, at the early stage of 3T3-L1 differentiation, the cells were treated with ET-1 (5 nM) for 48 h and then kept on differentiating for another 72 h. At the end of the experiment, differentiated adipocytes were stained with Oil Red O (Sigma-Aldrich, O0625). Simultaneously, intracellular triglyceride (TG) level was determined in the cells. The experiment was duplicated in different batches of cells.

Measurement of insulin-stimulated glucose uptake activity

To determine the glucose uptake activity in vitro, a fluorescent derivative of glucose, 2-(N-(7-Nitrobenz-2-oxa-1,3-diazol-4-yl)Amino)-2-Deoxyglucose (2-NBDG) (Invitrogen, N13195), was used as previously described with slight modifications⁶⁷. The differentiated primary isolated adipocytes were seeded onto 96-well plates using glucose-free media supplemented with 10% FBS and 1% antibiotics penicillin and streptomycin and incubated for 24 h in the presence or absence of 200 μ M PA. The cells were then stimulated with 100 nM insulin for 5 min and then incubated with medium containing 100 μ M 2-NBDG for

1 h at 37 °C. To stop 2-NBDG uptake, the incubation medium was removed, and the cells were washed twice with cold PBS. The fluorescence retained in cell was measured with a fluorescence microplate reader, setting at an excitation wavelength of 485 nm and emission wavelength of 535 nm.

Measurement of glucose-induced insulin release in β -cells and islets

The rat insulinoma cell line INS-1 832/13 was kindly provided by Dr. Chong Hyun Shin (Georgia State University, Atlanta, GA) and maintained as previously described⁶⁸. In brief, INS-1 832/13 cells were maintained in RPMI 1640 medium supplemented with 10% FBS, 1% antibiotics, 10 mM HEPES, 1 mM sodium pyruvate, and 50 μ M β -mercaptoethanol at 37 °C in a humidified 5% CO₂ atmosphere. To test the effect of ET-1, INS-1 832/13 cells were incubated with 5 nM ET-1 for 24 h. Then the medium was removed, and cells were washed with pre-warmed Krebs Ringer Buffer (KRB; containing 25 mM NaHCO₃, 4.64 mM KCL, 2.54 mM CaCl₂, 1.199 mM KH₂PO₄, 1.19 mM MgSO₄, 10 mM HEPES [pH 7.4]) and incubated with KRB containing 5, 10, 15, 25 mM glucose for 30 min. Each well was then aspirated and replaced with KRB containing the same concentrations of glucose and incubated for another 30 min. The supernatant was finally collected and assayed for insulin using an Insulin Rodent Chemiluminescence ELISA kit (ALPCO, 80-INSMR-CHO1).

To measure the ex vivo effect of ET-1 on insulin secretion, islets were isolated from mice according to previously described method⁶⁹. The captured islets (ten-size-matched islets were selected for each group) were cultured in Roswell Park Memorial Institute (RPMI) 1640 with 10% FBS and 1% antibiotics and treated with or without 5 nM ET-1 for 24 h. For the determination of dynamic insulin secretion, the isolated islets were incubated with KRB for 30 min and perfused with KRB containing 2.8 mM glucose for 5 min, and the perfusate was then switched to KRB containing 16.7 mM glucose. Eluted fractions were collected at 5-min intervals for 40 min. Insulin secreted in each fraction was measured using the insulin ELISA kit and normalized with total number of islets.

Measurement of lipid accumulation in hepatocytes and skeletal muscle cells

Human HepG2 hepatocytes and C2C12 myoblasts were kindly provided by Dr. Binghe Wang (Georgia State University, Atlanta, GA) and Dr. Hang Shi (Georgia State University, Atlanta, GA), respectively. Both HepG2 and C2C12 were grown in DMEM supplemented with 10% FBS and 1% antibiotics at 37 °C in 5% CO₂. For differentiation of C2C12 myoblasts, cells were grown to 100% confluence, transferred to differentiation medium (DMEM with 2% horse serum and 1% antibiotics), and fed with fresh differentiation medium every day for 3 days until myotubes were fully formed. To test the effect of ET-1 on ectopic lipid accumulation, HepG2 hepatocytes and C2C12 myotubes, respectively, were treated with or without 5 nM ET-1 for 24 h. The severity of lipid accumulation was then evaluated by determination of intracellular TG content and Oil red O staining according to the methods described previously⁷⁰.

Small interfering RNA (siRNA) transfection

HUVECs were transfected with scramble control siRNA or siRNA targeting *FUNDC1* (sc-91118, Santa Cruz Biotechnology), *SIRT3* (Santa Cruz Biotechnology, sc-61555), *GATA2* (Santa Cruz Biotechnology, sc-37228) using Lipofectamine-RNAiMAX transfection reagent (Life Technologies, 13778150) in Opti-MEM (Gibco, 31985) according to manufacturer's protocol.

Plasmid transfection

HUVECs were transfected with plasmids encoding *Myc-Flag*-tagged *FUNDC1* (Provided by Dr. Zhixue Liu) or *Flag*-tagged *SIRT3* (Addgene,

13814) using Lipofectamine-2000 transfection reagent (ThermoFisher, 11668019) in Opti-MEM according to manufacturer's protocol. The transfection efficiencies of the siRNAs and plasmids were determined by western blot analysis of target protein expression.

Subcellular fractionation

The subcellular fractionation was performed based on published protocols with slight modification⁷¹. HUVECs were harvested and homogenized by passing through a 27-gauge needle 10 times with fractionation buffer (150 mM KCl, 25 mM Tris pH 7.4, 5 mM EDTA, 0.5 mM protease inhibitors). The cell lysate was then centrifuged at 800 g for 10 min. The pellet was used as nucleus fraction (containing nuclear proteins). The supernatant (containing cytoplasmic, mitochondrial, and plasma-membrane proteins) was further purified by using Mitochondrial Isolation Kits (ThermoFisher, 89874) to get the mitochondrial fraction. Protein concentrations were determined using PierceTM BCA Protein Assay Kit (ThermoFisher Scientific, 23225) and equal amounts of proteins were subjected to immunoblotting analysis.

Immunoprecipitation

Immunoprecipitation (IP) analysis was performed as previously described⁶⁶. Briefly, proteins were isolated with IP lysis buffer (50 mM Tris, 40 mM NaCl, 1 mM EDTA, and 0.5% Triton, pH 7.4). Protein concentration was determined using PierceTM BCA Protein Assay Kit (ThermoFisher Scientific, 23225). 500 μ g of protein was incubated with antibodies against SIRT3 (Cell Signaling Technology, 5490), GATA2 (Novus, NBPI-82581), or acetylated-Lysine (Cell Signaling Technology, 9441) at 4 °C overnight. Immunoprecipitants were washed four times with lysis buffer, boiled in Laemmli buffer (Boston BioProducts, Inc., Ashland, MA) for 5 min, and analyzed by western blot.

Western blot

Tissues and cells were lysed in RIPA buffer. Protein was quantified using the BCA method (Pierce, USA). The lysates were resolved by SDS-PAGE and transferred to polyvinylidene difluoride membrane (Millipore Corp.). Membranes were probed with primary antibodies against FUNDC1 (Novus, NBPI-81063), ECE1 (Santa Cruz Biotechnology, sc-376018), GATA2 (Novus, NBPI-82581; Santa Cruz Biotechnology, sc-267), AP-1 (Cell Signaling Technology, 9165), SIRT3-L (LSBio, LS-C46967), SIRT3-S (Cell Signaling Technology, 5490), COX IV (Cell Signaling Technology, 4850), Lamin A/C (Cell Signaling Technology, 4777), ET-1 (Santa Cruz Biotechnology, sc-517436), p-AKT Ser473 (Cell Signaling Technology, 4060), AKT (Cell Signaling Technology, 4685), β -actin (Santa Cruz Biotechnology, 47778), or GAPDH (Santa Cruz Biotechnology, 32233), and subsequently incubated with horseradish peroxidase-linked secondary antibodies. The signals were visualized using an enhanced chemiluminescence detection system. The intensity of individual bands was quantified with ImageJ software (NIH). Data are represented as mean intensity of bands from at least three independent experiments.

Histology

Different adipose depots and aortas were collected, fixed in 4% paraformaldehyde overnight, and embedded in paraffin. The fixed tissues were sectioned into 4 μ m slides, and the slides were subjected to Haematoxylin and Eosin (H&E) staining, Elastic Verhoeff Van Gieson, or Collagen Sirius Red staining as previously described⁷².

Immunohistochemistry

The aortic sections were incubated with FUNDC1 (Biorbyt, orb156964), 8-OHdG (abcam, ab62623), or ET-1 (Novus, NB300-526) antibody at 4 °C overnight and followed by incubation with EnVision[®] + Dual Link System-HRP (Dako Cytomation, 3468) and the signal was visualized using the Liquid DAB+ Substrate Chromogen System and imaged using an inverted phase contrast microscope (Nikon, Tokyo, Japan). The

staining density and area in EC layer (the area between lumen and internal elastic layer) and adipose tissue were measured using ImageJ software (NIH).

Immunofluorescence staining

Immunofluorescence staining in HUVECs were performed by incubating the methanol-fixed cells with primary antibodies against FUNDC1 (Biorbyt, orb156964), SIRT3 (Santa Cruz Biotechnology, sc-365175), GATA2 (Proteintech, 11103-1-AP), or isotype control at 4 °C overnight, and followed by incubation with corresponding fluorescent secondary antibodies (Life Technologies) at room temperature for 1 h. Nuclei were stained with 4′6-diamidino-2-phenylindole (DAPI; Sigma-Aldrich, D9542). Images were captured by confocal laser scanning microscopy (LSM700, Carl Zeiss Co., Germany). Three independent experiments were performed and at least 3 high-power fields were analyzed for each experiment. Co-localization stains of FUNDC1 and SIRT3 were quantitated using the Pearson’s coefficient provided by the Zeiss software. Density and area of nuclear SIRT3 were measured using ImageJ software (NIH).

To quantitatively assess adipose tissue angiogenesis, fresh subcutaneous white adipose tissue (SubWAT) samples were prepared as whole-mount, paraffin-embedded sections and stained with the EC-specific marker CD31, as previously described⁷³. Briefly, adipose depots were fixed in 4% paraformaldehyde at 4 °C overnight, then cut into thin slices (5 mm × 5 mm). The slices were digested with 20 µg/mL proteinase K in 10 mM Tris-HCl buffer (pH 7.4) at room temperature for 5 min, followed by incubation in 100% methanol at room temperature for 30 min. Tissues were thoroughly washed in PBS for 1 h and then blocked with 3% blocking buffer (prepared from fat-free milk powder) at 4 °C for 24 h on a rocking platform. After extensive washing with PBST, samples were incubated with a monoclonal rabbit anti-mouse CD31 primary antibody (1:200 in PBST) for 24 h at 4 °C with rocking. Following removal of the primary antibody by thorough PBST washes, tissues were incubated with a goat anti-rabbit secondary antibody (1:400) for 2 hours at room temperature. To visualize adipocyte size, samples were stained with Bodipy (1:200 in PBS) for 30 minutes at room temperature. After overnight washing in PBST at 4 °C, tissues were mounted, and 3D images were acquired using confocal laser scanning microscopy. Quantitative image analysis was performed using ImageJ software.

Quantitative real time polymerase chain reaction (RT-PCR)

The intimal RNA was isolated from mouse thoracic aortas by flushing the lumen of aorta with TRIzol following an established method⁷⁴. Briefly, the lumen of thoracic aorta was quickly flushed (few seconds) with 200 µL of TRIzol reagent (Invitrogen) using a 29-gauge insulin syringe in a microfuge tube. The eluate was used for intimal RNA isolation by using a RNeasy Mini Kit (#74106, QIAGEN) according to the manufacturer’s instructions. For reverse transcription, cDNA was synthesized using iScript™ cDNA Synthesis Kit (Bio-Rad Laboratories, #170-8891). Primers used for gene amplification are shown in Supplementary Table. Quantitative RT-PCR reactions were performed using iQ™ SYBR® Green Supermix Kit (Bio-Rad Laboratories, 1708880) and a CFX96™ real-time system (Bio-Rad Laboratories) as described previously⁷⁵. Quantified results were represented using the 2^{-ΔΔCt} method with GAPDH as an internal control.

Tube formation assay and SA β-galactosidase assay

The EC tube formation assay was performed as previously described with slight modifications⁶⁶. Briefly, primary cultured ATECs were seeded into 96-well plates pre-coated with Matrigel (50 µL/well) at a density of 1.5 × 10⁴ cells/well in EBM supplemented with 20% FBS. Cells were treated with either vehicle or VEGF (50 ng/mL) and incubated at 37 °C for 24 h. Tube formation was observed and imaged using an inverted microscope (Olympus IX73, Tokyo, Japan). Quantification was

performed by counting the number of intersections in three randomly selected fields per well. To assess cellular senescence in vitro, primary ATECs were seeded in 12-well plates and treated with BSA (control) or 200 µM PA for 7 days. Cells were then fixed and stained using a senescence-associated β-galactosidase (SA-β-gal) staining kit (Cell Signaling Technology, catalog no. 9860), following the manufacturer’s instructions. Senescent cells were identified as SA-β-gal-positive (blue-stained) cells and imaged under a light microscope.

Statistics

Statistical analyses for data were performed using SPSS version 24.0 (IBM Corporation, Armonk, NY) and GraphPad Prism 8 (GraphPad Software, La Jolla, CA). For comparisons between two groups, significance was assessed using unpaired two-tailed Student’s *t*-tests, unpaired *t*-test with Welch’s correction or Mann Whitney test. For comparisons among multiple groups, analysis of variance (ANOVA) or appropriate nonparametric tests were applied to analyze the difference. All the data were expressed as mean ± standard deviation (SD). A *p*-value less than 0.05 was considered statistically significant.

Reporting summary

Further information on research design is available in the Nature Portfolio Reporting Summary linked to this article.

Data availability

All data supporting the conclusions of this study are included in the main text and supplementary materials. Additional datasets generated and analyzed during the current work are available from the corresponding author upon reasonable request. Source data are supplied with the published article. Source data are provided with this paper.

References

- Ogurtsova, K. et al. IDF Diabetes Atlas: global estimates for the prevalence of diabetes for 2015 and 2040. *Diab. Res. Clin. Pract.* **128**, 40–50 (2017).
- Collaboration, N. R. F. Trends in adult body-mass index in 200 countries from 1975 to 2014: a pooled analysis of 1698 population-based measurement studies with 19.2 million participants. *Lancet* **387**, 1377–1396 (2016).
- Prieto, D., Contreras, C. & Sánchez, A. Endothelial dysfunction, obesity and insulin resistance. *Curr. Vasc. Pharmacol.* **12**, 412–426 (2014).
- Engin, A. Endothelial dysfunction in obesity. *Obesity Lipotoxicity*, 345–379 (2017).
- Li, M., Qian, M., Kyler, K. & Xu, J. Adipose tissue-endothelial cell interactions in obesity-induced endothelial dysfunction. *Front. Cardiovasc. Med.* 646 (2021).
- Bakker, W., Eringa, E. C., Sipkema, P. & van Hinsbergh, V. W. Endothelial dysfunction and diabetes: roles of hyperglycemia, impaired insulin signaling and obesity. *Cell tissue Res.* **335**, 165–189 (2009).
- Bonetti, P. O., Lerman, L. O. & Lerman, A. Endothelial dysfunction: a marker of atherosclerotic risk. *Arterioscl. Thromb. Vasc. Biol.* **23**, 168–175 (2003).
- Amiri, F. et al. Endothelium-restricted overexpression of human endothelin-1 causes vascular remodeling and endothelial dysfunction. *Circulation* **110**, 2233–2240 (2004).
- Naderi-Meshkin, H. & Setyaningsih, W. A. W. Endothelial cell dysfunction: onset, progression, and consequences. *Front. Biosci. Landmark* **29**, 223 (2024).
- Peng, Z., Shu, B., Zhang, Y. & Wang, M. Endothelial response to pathophysiological stress. *Arterioscl. Thromb. Vasc. Biol.* **39**, e233–e243 (2019).
- Guzik, T. J. & Touyz, R. M. Oxidative stress, inflammation, and vascular aging in hypertension. *Hypertension* **70**, 660–667 (2017).

12. Lien, C. C. et al. Chronic endothelin-1 infusion causes adipocyte hyperplasia in rats. *Obesity* **24**, 643–653 (2016).
13. Wilkes, J. J., Hevener, A. & Olefsky, J. Chronic endothelin-1 treatment leads to insulin resistance in vivo. *Diabetes* **52**, 1904–1909 (2003).
14. Hauner, H., Petruschke, T. & Gries, F. Endothelin-1 inhibits the adipose differentiation of cultured human adipocyte precursor cells. *Metabolism* **43**, 227–232 (1994).
15. Feger, M. et al. Endothelin receptor B-deficient mice are protected from high-fat diet-induced metabolic syndrome. *Mol. Metab.* **80**, 101868 (2024).
16. Koenen, M., Hill, M. A., Cohen, P. & Sowers, J. R. Obesity, adipose tissue and vascular dysfunction. *Circ. Res.* **128**, 951–968 (2021).
17. Jenkins, H. N., Rivera-Gonzalez, O., Gibert, Y. & Speed, J. S. Endothelin-1 in the pathophysiology of obesity and insulin resistance. *Obes. Rev.* **21**, e13086 (2020).
18. Biswas, S. et al. Endothelin-1 regulation is entangled in a complex web of epigenetic mechanisms in diabetes. *Physiol. Res.* **67** (2018).
19. Hammarstedt, A., Gogg, S., Hedjazifar, S., Nerstedt, A. & Smith, U. Impaired adipogenesis and dysfunctional adipose tissue in human hypertrophic obesity. *Physiol. Rev.* **98**, 1911–1941 (2018).
20. Wu, S. et al. Hyperglycemia-driven inhibition of AMP-activated protein kinase $\alpha 2$ induces diabetic cardiomyopathy by promoting mitochondria-associated endoplasmic reticulum membranes in vivo. *Circulation* **139**, 1913–1936 (2019).
21. Wu, S. et al. Binding of FUN14 domain containing 1 with inositol 1, 4, 5-trisphosphate receptor in mitochondria-associated endoplasmic reticulum membranes maintains mitochondrial dynamics and function in hearts in vivo. *Circulation* **136**, 2248–2266 (2017).
22. Wang, C. et al. FUNDC1-dependent mitochondria-associated endoplasmic reticulum membranes are involved in angiogenesis and neoangiogenesis. *Nat. Commun.* **12**, 2616 (2021).
23. Liu, L. et al. Mitochondrial outer-membrane protein FUNDC1 mediates hypoxia-induced mitophagy in mammalian cells. *Nat. cell Biol.* **14**, 177–185 (2012).
24. Cao, Y., Wang, H., Wang, Q., Han, X. & Zeng, W. Three-dimensional volume fluorescence-imaging of vascular plasticity in adipose tissues. *Mol. Metab.* **14**, 71–81 (2018).
25. Ramakrishnan, V. M. & Boyd, N. L. The adipose stromal vascular fraction as a complex cellular source for tissue engineering applications. *Tissue Eng. Part B Rev.* **24**, 289–299 (2018).
26. Kizhakekuttu, T. J. et al. Adverse alterations in mitochondrial function contribute to type 2 diabetes mellitus-related endothelial dysfunction in humans. *Arterios. Thromb. Vasc. Biol.* **32**, 2531–2539 (2012).
27. Pellegrinelli, V., Rouault, C., Veyrie, N., Clément, K. & Lacasa, D. Endothelial cells from visceral adipose tissue disrupt adipocyte functions in a three-dimensional setting: partial rescue by angiotensin-1. *Diabetes* **63**, 535–549 (2014).
28. Fukumura, D. et al. Paracrine regulation of angiogenesis and adipocyte differentiation during in vivo adipogenesis. *Circ. Res.* **93**, e88–e97 (2003).
29. Weil, B. R. et al. Enhanced endothelin-1 system activity with overweight and obesity. *Am. J. Physiol. Heart Circ. Physiol.* **301**, H689–H695 (2011).
30. Musarò, A., McCullagh, K. J., Naya, F. J., Olson, E. N. & Rosenthal, N. IGF-1 induces skeletal myocyte hypertrophy through calcineurin in association with GATA-2 and NF-ATc1. *Nature* **400**, 581–585 (1999).
31. Komatsu, M. et al. Cell-cycle dependent GATA2 subcellular localization in mouse 2-cell embryos. *Biochem. Biophys. Res. Commun.* **584**, 1–6 (2021).
32. Lionaki, E., Gkikas, I. & Tavernarakis, N. Differential protein distribution between the nucleus and mitochondria: implications in aging. *Front. Genet.* **7**, 162 (2016).
33. Scher, M. B., Vaquero, A. & Reinberg, D. SirT3 is a nuclear NAD⁺-dependent histone deacetylase that translocates to the mitochondria upon cellular stress. *Genes Dev.* **21**, 920–928 (2007).
34. Schwer, B., North, B. J., Frye, R. A., Ott, M. & Verdin, E. The human silent information regulator (Sir) 2 homologue hSIRT3 is a mitochondrial nicotinamide adenine dinucleotide-dependent deacetylase. *J. Cell Biol.* **158**, 647–657 (2002).
35. Yang, L. et al. SIRT3 deficiency induces endothelial insulin resistance and blunts endothelial-dependent vasorelaxation in mice and human with obesity. *Sci. Rep.* **6**, 1–12 (2016).
36. Hirschey, M. D. et al. SIRT3 deficiency and mitochondrial protein hyperacetylation accelerate the development of the metabolic syndrome. *Mol. cell* **44**, 177–190 (2011).
37. Hayakawa, F. et al. Functional regulation of GATA-2 by acetylation. *J. Leukoc. Biol.* **75**, 529–540 (2004).
38. Guan, K.-L. & Xiong, Y. Regulation of intermediary metabolism by protein acetylation. *Trends Biochem. Sci.* **36**, 108–116 (2011).
39. Choudhary, C. et al. Lysine acetylation targets protein complexes and co-regulates major cellular functions. *Science* **325**, 834–840 (2009).
40. Li, Y. et al. A mitochondrial FUNDC1/HSC70 interaction organizes the proteostatic stress response at the risk of cell morbidity. *EMBO J.* **38**, e98786 (2019).
41. Wang, C. et al. FUNDC1-dependent mitochondria-associated endoplasmic reticulum membranes are involved in angiogenesis and neoangiogenesis. *Nat. Commun.* **12**, 1–13 (2021).
42. Corvera, S. & Gealekman, O. Adipose tissue angiogenesis: impact on obesity and type-2 diabetes. *Biochim. Biophys. Acta Mol. Basis Dis.* **1842**, 463–472 (2014).
43. Ferri, C. et al. Circulating endothelin-1 levels in obese patients with the metabolic syndrome. *Exp. Clin. Endocrinol. Diab.* **105**, 38–40 (1997).
44. Maeda, S. et al. Weight loss reduces plasma endothelin-1 concentration in obese men. *Exp. Biol. Med.* **231**, 1044–1047 (2006).
45. Juan, C.-C. et al. Endothelin-1 induces insulin resistance in conscious rats. *Biochem. Biophys. Res. Commun.* **227**, 694–699 (1996).
46. Ottosson-Seeberger, A., Lundberg, J., Alvestrand, A. & Ahlborg, G. Exogenous endothelin-1 causes peripheral insulin resistance in healthy humans. *Acta Physiol. Scand.* **161**, 211–220 (1997).
47. Piatti, P. et al. Relationship between endothelin-1 concentration and metabolic alterations typical of the insulin resistance syndrome. *Metabolism* **49**, 748–752 (2000).
48. Juan, C.-C., Chang, C.-L., Lai, Y.-H. & Ho, L.-T. Endothelin-1 induces lipolysis in 3T3-L1 adipocytes. *Am. J. Physiol. Endocrinol. Metab.* **288**, E1146–E1152 (2005).
49. Eriksson, A. et al. Endothelin-1 stimulates human adipocyte lipolysis through the ETA receptor. *Int. J. Obes.* **33**, 67–74 (2009).
50. van Harmelen, V. et al. Vascular peptide endothelin-1 links fat accumulation with alterations of visceral adipocyte lipolysis. *Diabetes* **57**, 378–386 (2008).
51. Heimlich, J. B. et al. ET-1 increases reactive oxygen species following hypoxia and high-salt diet in the mouse glomerulus. *Acta Physiol.* **213**, 722–730 (2015).
52. Weir, H. J., Lane, J. D. & Balthasar, N. SIRT3: a central regulator of mitochondrial adaptation in health and disease. *Genes Cancer* **4**, 118–124 (2013).
53. Sundaresan, N. R., Samant, S. A., Pillai, V. B., Rajamohan, S. B. & Gupta, M. P. SIRT3 is a stress-responsive deacetylase in cardiomyocytes that protects cells from stress-mediated cell death by deacetylation of Ku70. *Mol. Cell. Biol.* **28**, 6384–6401 (2008).
54. Ren, J. et al. FUNDC1 interacts with FBXL2 to govern mitochondrial integrity and cardiac function through an IP3R3-dependent manner in obesity. *Sci. Adv.* **6**, eabc8561 (2020).

55. Ansari, A. et al. Function of the SIRT3 mitochondrial deacetylase in cellular physiology, cancer, and neurodegenerative disease. *Aging Cell* **16**, 4–16 (2017).
56. Ahn, B.-H. et al. A role for the mitochondrial deacetylase Sirt3 in regulating energy homeostasis. *Proc. Natl. Acad. Sci. USA* **105**, 14447–14452 (2008).
57. Williams, L. M. et al. The development of diet-induced obesity and glucose intolerance in C57BL/6 mice on a high-fat diet consists of distinct phases. *PLoS one* **9**, e106159 (2014).
58. Ruppert, Z. et al. Characterization of obesity-related diseases and inflammation using single cell immunophenotyping in two different diet-induced obesity models. *Int. J. Obes.* **48**, 1568–1576 (2024).
59. Fewkes, J. J., Kellow, N. J., Cowan, S. F., Williamson, G. & Dordevic, A. L. A single, high-fat meal adversely affects postprandial endothelial function: a systematic review and meta-analysis. *Am. J. Clin. Nutr.* **116**, 699–729 (2022).
60. Chen, L. et al. Saturated fatty acids increase LPI to reduce FUNDC1 dimerization and stability and mitochondrial function. *EMBO Rep.* **24**, e54731 (2023).
61. Dai, X. et al. Ablation of Neuropilin 1 in Myeloid Cells Exacerbates High-Fat Diet-Induced Insulin Resistance Through Nlrp3 Inflammation In Vivo. *Diabetes* **66**, 2424–2435 (2017).
62. Ding, Y. et al. Peroxynitrite-mediated SIRT (Sirtuin)-1 inactivation contributes to nicotine-induced arterial stiffness in mice. *Arterioscler. Thromb. Vasc. Biol.* **39**, 1419–1431 (2019).
63. Wang, Q. et al. Metformin suppresses diabetes-accelerated atherosclerosis via the inhibition of Drp1-mediated mitochondrial fission. *Diabetes* **66**, 193–205 (2017).
64. Kumarathasan, P., Goegan, P. & Vincent, R. An automated high-performance liquid chromatography fluorescence method for the analyses of endothelins in plasma samples. *Anal. Biochem.* **299**, 37–44 (2001).
65. Saleh, M. A., Boesen, E. I., Pollock, J. S., Savin, V. J. & Pollock, D. M. Endothelin-1 increases glomerular permeability and inflammation independent of blood pressure in the rat. *Hypertension* **56**, 942–949 (2010).
66. Yao, H. et al. Ablation of endothelial Atg7 inhibits ischemia-induced angiogenesis by upregulating Stat1 that suppresses Hif1a expression. *Autophagy* (2022).
67. Zhang, Y. et al. Hypoglycemic activity evaluation and chemical study on hollyhock flowers. *Fitoterapia* **102**, 7–14 (2015).
68. Jia, Y.-F. et al. TBK1 regulates regeneration of pancreatic β -cells. *Sci. Rep.* **10**, 19374 (2020).
69. Wang, B. et al. The adaptor protein APPL2 controls glucose-stimulated insulin secretion via F-actin remodeling in pancreatic β -cells. *Proc. Natl. Acad. Sci. USA* **117**, 28307–28315 (2020).
70. Li, J. et al. Inhibitory effects of constituents from the aerial parts of *Rosmarinus officinalis* L. on triglyceride accumulation. *Molecules* **22**, 110 (2017).
71. Han, Y.-M. et al. β -Hydroxybutyrate prevents vascular senescence through hnRNP A1-mediated upregulation of Oct4. *Mol. Cell* **71**, 1064–1078.e1065 (2018).
72. Li, J. et al. Pycard deficiency inhibits microRNA maturation and prevents neointima formation by promoting chaperone-mediated autophagic degradation of AGO2/argonaute 2 in adipose tissue. *Autophagy* **20**, 629–644 (2024).
73. Xue, Y., Lim, S., Bråkenhielm, E. & Cao, Y. Adipose angiogenesis: quantitative methods to study microvessel growth, regression and remodeling in vivo. *Nat. Protoc.* **5**, 912–920 (2010).
74. Nam, D. et al. Partial carotid ligation is a model of acutely induced disturbed flow, leading to rapid endothelial dysfunction and atherosclerosis. *Am. J. Physiol. Heart Circ. Physiol.* **297**, H1535–H1543 (2009).
75. Ouyang, C. et al. Deletion of Ulk1 inhibits neointima formation by enhancing KAT2A/GCN5-mediated acetylation of TUBA/ α -tubulin in vivo. *Autophagy* **17**, 4305–4322 (2021).

Acknowledgements

This work was supported in part by funding from the National Heart, Lung, and Blood Institute HL153333 (Y.D), American Heart Association 19CDA34730035 (Y.D), and American Heart Association Transformational Award 970764 (M.H. Zou). This work was also supported in part by National Natural Science Foundation of China (82470443 and 82530049 to M.H.Z.). We greatly appreciate Dr. Zhonglin Xie for his in-depth discussion and advice.

Author contributions

M.-H.Z. and Y.D. conceived the project. M.-H.Z. and J.L. designed the study and wrote the manuscript. J.L., D.L., F.Z., H.Y., Ya.W., Yi.W., J.A., and Z.L. carried out all the experiments and analyzed data. M.-H.Z. and Y.D. supervised experiments and interpreted results. M.-H.Z. and Y.D. obtained funding for this study. All authors had final approval of the submitted and published versions.

Competing interests

The authors declare no competing interests.

Additional information

Supplementary information The online version contains supplementary material available at <https://doi.org/10.1038/s41467-026-68548-4>.

Correspondence and requests for materials should be addressed to Ye Ding or Ming-Hui Zou.

Peer review information *Nature Communications* thanks the anonymous reviewer(s) for their contribution to the peer review of this work. A peer review file is available.

Reprints and permissions information is available at <http://www.nature.com/reprints>

Publisher's note Springer Nature remains neutral with regard to jurisdictional claims in published maps and institutional affiliations.

Open Access This article is licensed under a Creative Commons Attribution-NonCommercial-NoDerivatives 4.0 International License, which permits any non-commercial use, sharing, distribution and reproduction in any medium or format, as long as you give appropriate credit to the original author(s) and the source, provide a link to the Creative Commons licence, and indicate if you modified the licensed material. You do not have permission under this licence to share adapted material derived from this article or parts of it. The images or other third party material in this article are included in the article's Creative Commons licence, unless indicated otherwise in a credit line to the material. If material is not included in the article's Creative Commons licence and your intended use is not permitted by statutory regulation or exceeds the permitted use, you will need to obtain permission directly from the copyright holder. To view a copy of this licence, visit <http://creativecommons.org/licenses/by-nc-nd/4.0/>.

© The Author(s) 2026